CAMBRIDGE UNIVERSITY

MASTER'S PROJECT

Characterisation and interpretation of austenite grain growth kinetics in an advanced nuclear pressure vessel steel

Ailsa A Kiely

A thesis presented for the degree of
Masters of Philosophy

Department of Materials Science and Metallurgy
Jesus College
University of Cambridge
United Kingdom
26th October 2016

Abstract

A nuclear pressure vessel steel desginated "Grade 4N" has been high-lighted as a potential new candidate for fourth generation reactor pressure vessels. Previous research on austenite grain growth in a conventional steel (Grade 3) has been undertaken but new requirements are for a tougher variant. Toughness depends critically on austenite grain growth, which has not been studied in the Grade 4N alloy. The focus of this work presented here is therefore the characterisation of the austenite grain growth in the new alloy. High temperature techniques, such as Dilatometry, was utilised to thermally groove polished samples due to surface tension at the austenite grain boundaries so they could easily be measured. It was discovered that whereas Grade 3 alloy displayed significant Zener pinning of grain boundaries due to aluminium nitride, the Grade 4N grains continued to grow with no pinning effects being displayed. The grain size of the new alloy can therefore be larger than in the conventional alloy, which may cause a deterioration in mechanical properties. The probable reason for this is its much smaller concentration of aluminium so this needs to be assessed in future work. The present results nevertheless are of considerable importance in the context of heat affected zones of electron beam welds where austenite growth during the transient heat pulse must be managed.

Declaration of Authorship

I, Ailsa Anne Kiely, declare that this thesis titled, Characterisation and interpretation of austenite grain growth kinetics in an advanced nuclear pressure vessel steel, and the work presented in it are my own. I confirm that:

- This work was done wholly or mainly while in candidature for a research degree at this University.

- Where any part of this thesis has previously been submitted for a degree or any other qualification at this University or any other institution, this has been clearly stated.

- Where I have consulted the published work of others, this is always clearly attributed.

- Where I have quoted from the work of others, the source is always given. With the exception of such quotations, this thesis is entirely my own work.

- I have acknowledged all main sources of help.

- Figures 1.1 and 1.2 are reproduced here under creative license commons

- Where the thesis is based on work done by myself jointly with others, I have made clear exactly what was done by others and

what I have contributed myself.

Signed:

_____

Date:

_____

Acknowledgements

I would like to thank my supervisor, Professor Harry Bhadeshia for his constant guidance, motivation and constructive feedback allowing me to enrich my knowledge. I would also like to thank Dr. Pous-Romero and Dr. Cogswell who have been thoroughly supportive and provided useful insight into this area of research.

Further, I would like to thank the members of the Phase Transformations and Complex Properties Research Group for their help, suggestions and support, especially Dr Chris Hulme-Smith, Arunim Ray and Neelabhro Bhattacharya who did not hesitate to offer valuable time, assistance and understanding. I am especially grateful to Dr Ed Pickering who scrutinised my work and provided exceptional editing assistance along with answering my many questions.

Additionally I would like to thank Dr Mathew Peet and Kevin Roberts for their constant assistance and advice with the Thermecmastor-Z.

Aside from this academic support, I would like to thank friends and family at this time who have provided encouragement and moral support.I would like especially to thank my good friends Leanne Greenfield, Lucy Morgan, James Pascoe, Taegyn Turnley, Fergus Vickery and Lydia Woodward who put up with my long scientific conversations de-

spite being humanties students.

Contents

1 — Introduction

1.2 Motivation

With fossil fuel supply diminishing and renewables still in their relatively early stages of mass implementation, nuclear energy is becoming increasingly important as a potential energy source to meet carbon dioxide emission targets. As a result of the strict safety and other requirements for nuclear reactor pressure vessels (RPVs), only a few steels have been approved for this application. These alloys have undergone rigorous testing over a long period of time prior to application. ASME SA508 is an alloy which currently fulfils the necessary requirements in service and has been utilised for decades due to the acceptable compromise between strength, toughness and cost [1-4].

SA508 has a broad specification and comprises numerous classes of slightly varying composition.

1.2.1 Current material

SA508 Grade 3 steel is currently utilised for Generation III reactor pressure vessels due to its superior mechanical properties compared to earlier alloys. Recent research has focused on the austenitising process of these steels. This crucial stage in achieving an optimum grain size has a

direct effect on the hardenability and final properties of the components which are necessarily very large [3].

However with the nuclear energy industry now looking for a reactor service life in excess of 60 years and requiring higher tensile strength, toughness and resistance to irradiation embrittlement, there is demand for a new candidate material for application in the next Generation IV plants. One such candidate alloy is SA508 Grade 4N, the focus of this research.

1.2.2   Problem statement

As the RPV is the critical life limiting component any new material must demonstrate increased durability, toughness and strength. RPVs operate under extreme conditions at high temperatures, stresses, in corrosive environments and with neutron irradiation. These conditions mean that the structural materials chosen must have exceptional properties. Under standard operating conditions most pressurised water reactors function at between 270° C and 330° C under a large pressure of 15 MPa [26,37].

Strict regulations are imposed on the nuclear energy industry to minimise the probabilities of failure of these critical components; hence the safety margin requirements ensure that the materials utilised have the necessary properties to withstand premature failure [3,26,37].

SA508 Grade 4N apparently has enhanced mechanical properties compared to SA508 Grade 3 currently in use. However there are few experimental data from in-service applications. As microstructure is crucial to

a components properties and with the short time frame available until construction of generation IV plants, there is pressure to undertake microstructural and characterisation investigations of this candidate material [37]. In particular to fully understand the effect of heat treatments on the microstructure.

The main objective of this research was to investigate the effect of varying austenitising temperatures and times on the microstructure as compared to the current Grade 3 material. This aim was accomplished through the use of thermodynamic modelling and experimental investigation utilising dilatometry. The phase diagram calculations helped estimate whether any pinning phases would be present at varying austenitising temperatures and holding times. Dilatometry was used to thermally etch the samples for measurement of the austenite grain size. The experimental results were analysed against the prediction of pinning particles.

1.2.3 Thesis organisation

Following this Introduction, Chapter 2 provides an overview of current literature; a brief review of nuclear energy and nuclear reactors, examining changes in the material used. In particular, attention is paid to the fabrication of the current material utilised in the manufacture of RPVs, specifically highlighting the heat treatment stages. The modelling of austenite grain growth and thermal grooving theory are discussed. This chapter evidences through examination of the literature that there is a significant lack of information available for SA508 Grade 4N.

Chapter 3 outlines the experimental method employed for the analysis

of the prior austenite grain size. A brief discussion of the utilisation of MT-DATA thermodynamic software and in depth analysis of size predictive model indicates that in theory pinning is unlikely to occur [3,43]. This hypothesis is then tested through experimental work.

Both the modelling results and experimental findings are presented in Chapter 4.

Chapter 5 provides an evaluation of both the modelling and experimental findings. Additional future work is proposed in order to fully characterise the potential for application as an RPV material.

2 — Literature Review

2.1 History of nuclear energy

The first developments towards nuclear energy were brought to the attention of the scientific community in the early part of the 20th century. Experiments undertaken in 1911 by Ernst Rutherford found that when radium atoms decayed there was a substantial evolution of heat leading to the hypothesis that atoms were stores of energy [1-3]. Simultaneously, Einstein demonstrated that mass and energy were in equivalence with the famous equation 2.1 [4]:

$$E = mc^2 \qquad (2.1)$$

where E represents energy, m represents mass and c is the speed of light. These two scientific hypothesises paved the way for nuclear research.

However the scientific community faced a conundrum with regard to the extraction of this energy until the discovery of fission. In 1934 experiments conducted by Enrico Fermi (Figure 2.1) illustrated that a significant number of elements could be transformed by neutron bombardment [5-7]. These experiments were based on the fundamental findings that an atom contained a nucleus and that a nucleus comprises of protons and neutrons. At this time the periodic table was not in the same format as today which led to unexplainable findings upon neu-

tron bombardment of uranium with two lighter products being produced [8-10]. It was not until April 1939, that six research groups worldwide confirmed the concept of fission [8].

Figure 2.1: Enrico Fermi at Chicago University [11].

Two groups at Columbia University under Fermi's guidance published work determining that fission occurs when a neutron is captured by a heavy parent nuclei, such as uranium-235 (U^{235}), leading this to become unstable [8, 12]. This unstable parent nucleus subsequently degrades producing two lighter fission fragments, barium and krypton, with the release of two or three neutrons and 200 MeV of kinetic energy [13].

The two smaller nuclei that are formed have a combined mass less than that of the original parent nuclei and thus energy is created forming a mass defect. Using Einstein's mass-energy equivalence equation (Equation 2.1) the kinetic energy can be calculated from the mass defect [13,14].

As uranium-235 (U^{235}) is the most common fuel stock, a fission reaction would occur as follows [14]:

$$\ce{^{235}_{92}U} + \ce{^{1}_{0}}n \rightarrow \ce{^{236}_{92}U} \rightarrow \ce{^{143}_{56}Ba} + \ce{^{90}_{36}Kr} + 3\ce{^{1}_{0}}n \qquad (2.2)$$
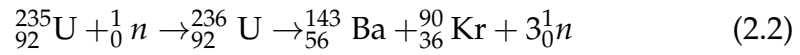
The scientific community was quick to realise the potential of the energy released upon fission. In 1939 the use of uranium as a fuel stock and graphite as a moderator confirmed that neutrons evolved upon fission were generated in a large enough numbers to achieve a self sustaining chain reaction through multiple scattering collisions [1,13].

Figure 2.2: Chicago Pile -1 [8].
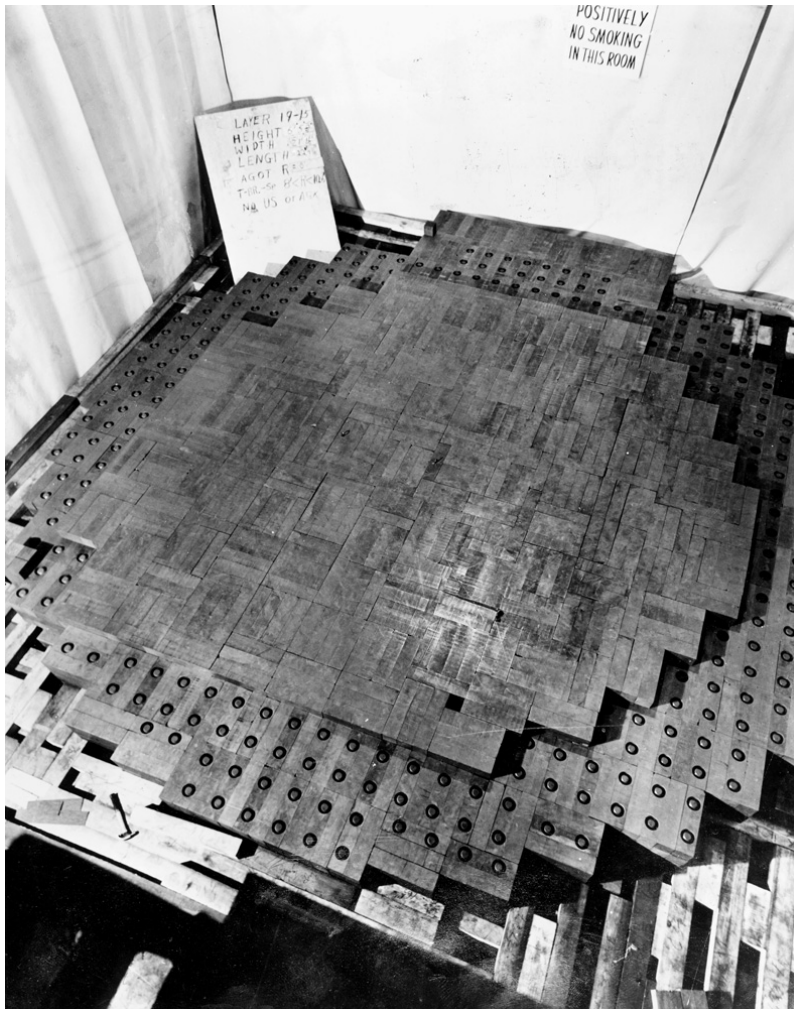
In August 1939, the second World War accelerated research with the

first utilisation of fission being for military application rather than the initial peaceable applications intended. In 1942 world leading scientists led by Fermi at the University of Chicago proceeded to discuss the manufacture of the first controllable chain-reaction nuclear reactor named the Chicago Pile -1 (Figure 2.2). The Manhattan Project was established in 1942 and had the main aim of producing plutonium- 239, a by-product of fission, which could be used in the manufacture of a fission bomb. The Chicago Pile -1 reactor was found to have insufficient power, 200 W, to achieve this aim leading to the manufacture of a new 1 MW pilot plant, the X-10 Graphite Reactor [1,10].

Following the end of the second World War in 1945 the Atomic Energy Commission was created to construct the "Experimental Breeder Reactor 1" in Idaho. The first electricity from nuclear energy was produced on 20th December 1951 and the first commercial nuclear electricity plant reached full power in 1957 [1,3].

A rapid increase in the construction of nuclear power plants occurred in the 1950s to 1970s as nuclear energy was perceived as both safe and clean. Notably it provides a solution which lacks CO_2 emissions and has the potential for replacement of fossil fuels. This perception was subsequently challenged following a number of major catastrophes including Chernobyl in 1986, Windscale and Three-mile island with the more recent being Fukushima in 2011, resulting in negative public sentiment towards nuclear power even though no fatalities occurred [10].

Subsequent to the Fukushima disaster certain countries changed their nuclear policy due to public controversy over this energy source. Japan withdrew all support for nuclear power, however the reactors were

later reinstated, whilst Germany decommissioned half its nuclear power plants with the remainder set to be decommissioned by 2020 [15]. The UK and USA undertook intensive safety and risk assessments of their existing plants continuing to favour the use of nuclear power [16].

In recent years use of nuclear power has been debated frequently due to increased concerns regarding climate change, energy security and diminishing fossil fuels and price volatility in the energy market. Notably the UK's target of an 80 % reduction in carbon emissions by 2050 has resulted in renewed interest in nuclear energy to meet this target [17]. The International Atomic Energy Authority (IAEA) 2014 report indicates that there are 434 reactors in operation in 30 countries with two reactors permanently shut down and 72 reactors under construction [18]. With growing populations in China, India and other developing economies, the global electricity demand is hypothesised to double to more than 30,000 TWh by 2030. Notably Britain, France and China are investing in the next generation nuclear power stations in addition to updating their current plants to meet the increased energy demands [19]. Improving living standards will require a variety of technologies to meet growing global energy demands. Nuclear power provides a well-established scalable solution for generating electricity with no carbon emissions [3,19].

2.2   Nuclear reactors

Nuclear reactor design and technology have been undergoing developments for over five decades. The first Generation I Magnox reactors were built in the 1960s with Generation II, Pressurised water reactors and Advanced gas-cooled reactors, following from the 1970s with these

9

being the most common reactors currently in operation. By the 1990s Generation III reactors were being constructed with increased reliability and economics [1,3,20]. This generation of reactor has a simple design with greater safety features and increased mitigation measures against nuclear accidents. The main driving force for the development of the next generation of reactor is the need to increase the reactor's lifetime.

The two principal Generation III operating civil nuclear reactors are Pressurized Water Reactors (PWRs) and Boiling Water Reactors (BWRs) which in 2008 produced 66 % and 23 % of the world's nuclear energy, respectively. Notably both these reactor designs originate from U.S. naval technology specifically their nuclear submarine program [21-23]. As the majority of operational reactors are PWRs it is essential to optimise their design and materials for increased operational lifetime.

Figure 2.3 illustrates a schematic of a PWR plant. The PWR core consists of between 190 and 240 fuel assemblies within the Reactor Pressure Vessel (RPV) containing 90,000 kg of UO_2 fuel stock with dimensions of 3.5 m diameter by 4.0 m in height. Liquid coolant, with a pressure of 15 MPa and temperature 290°C, flows upwards between the inner wall and the core exiting at the top of the RPV. This primary coolant is present in an enclosed loop with the heat being passed through to a secondary coolant in the steam generator producing dry steam which is converted into mechanical energy in the turbine-generator upon expansion [24].

Significantly, the life of a nuclear reactor is determined by that of the limiting component, the reactor pressure vessel, which cannot be replaced during service due to irradiation. This occurs due to fast un-

Figure 2.3: Schematic of PWR reactor [25].
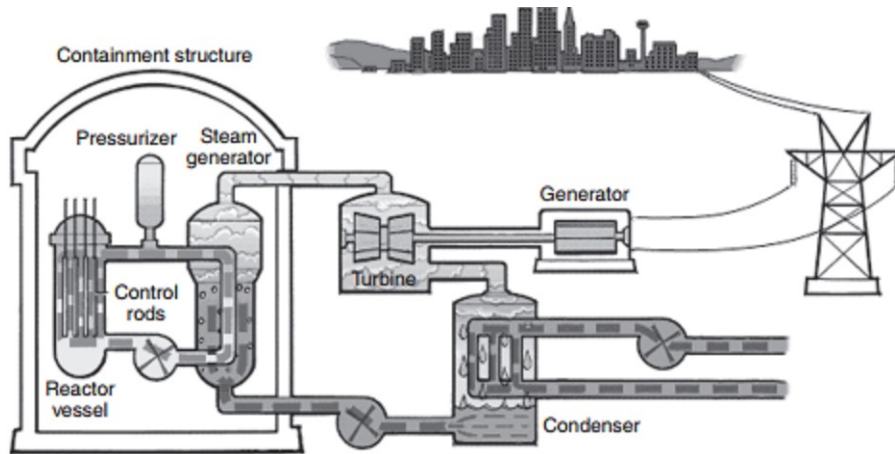
moderated neutrons, causing the steel, of which the RPV is constructed from, to become brittle [26]. Generation II reactors have an operating lifetime of 40 years and Generation III reactors 60 years. Currently Generation IV reactors are being designed for construction in the 2030's with a key industrial requirement being an extended lifetime in excess of 60 years [27]. Other requirements include improvements in economics, usage of natural resources and proliferation security [3]. Proliferation is where fission materials are obtained by countries that are not accepted as nuclear states leading to the potential production of nuclear weapons.

These new reactors will require materials with greater durability and toughness; as such the lifetime of these Generation IV reactors will be governed by the structural integrity and performance of the materials employed.

2.3   Current reactor pressure vessel materials

Current industrial requirements are that nuclear reactors should provide greater power capacity and a longer operational lifespan. Gener-

ation IV PWRs are based on modularised reactors, which are smaller and have greater capacity than the current Generation III. RPVs subject to degradation by neutron irradiation are the critical components that determine the life span and safety margin of nuclear reactors. It is imperative to understand the detailed characterisation of the properties of the materials which need to be of sufficient strength and toughness to prevent premature failure. Low alloy ferritic steels are the primary candidate with SA508 low-alloy steels being an ideal material [27-29].

The common code for the nuclear industry is produced by the American School of Mechanical Engineers (ASME). Notably SA508 specification section II from ASME allows for various chemical compositions grades that are sub-divided into classes based on varying heat treatments. The range of chemical compositions of the SA508 steels is outlined in Table 2.1 along with the mechanical properties in Table 2.2 [3, 30].

Table 2.1: Range of maximium chemical compositions of SA508 steels in wt.% [3, 30].

	Grade 1	Grade 2	Grade 3	Grade 4N
Carbon	0.35	0.27	0.25	0.23
Manganese	0.40-1.05	0.50-1.00	1.20-1.50	0.20-0.40
Nickel	0.40	0.50-1.00	0.4-1.00	2.8-3.9
Chromium	0.25	0.25-0.45	0.25	1.5-2.00
Molybednum	0.10	0.55-0.70	0.45-0.60	0.40-0.60
Silicon	0.15-0.35	0.15-0.35	0.15-0.35	0.15
Sulphur	0.025	0.025	0.025	0.025
Phosphorus	0.025	0.025	0.025	0.025
Vanadium	0.005	0.005	0.005	0.005

Table 2.2: Mechanical Properties for varying alloy composition for SA508 [3, 30].

	Tensile strength / MPa	Yield strength / MPa	Elongation /%
SA508 Grade 1	345	515	16
SA508 Grade 2	611	448	18
SA508 Grade 3	611	468	29
SA508 Grade 4N	725	585	18

Research has ascertained that controlling the heat treatment conditions and chemical composition can help to optimise the mechanical properties, such as strength,toughness and weldability, of RPV materials [28, 29]. RPVs currently in service are manufactured from SA508 Grade 3. This material provides radiation resistance for up to 40 years with a yield strength of over 345 MPa. However, Grade 3 is not appropriate for Generation IV nuclear plants which have a required lifespan in excess of 60 years [30,31]. This is due to the material constraints as Grade 3 lifetime is less than 60 years as a result of irradiation embrittlement [3,38].

To meet the industry's requirements going forward, a new nickel-rich steel, SA508 Grade 4N is proposed with enhanced strength and toughness compared to Grade 3 and which it is predicted will increase the safety and economics of RPVs [32]. With the increased nickel content a significant increase in yield strength of 25% is observed with the fracture toughness also being improved substantially through the optimisation of the chemical composition [28].

The nuclear industry notably relies on extensive experimental databases in order to confirm the ability of a material to perform in service. However, there is a lack of experimental data in relation to Grade 4N steel in

service, particularly regarding irradiation embrittlement and welding properties over long term operation. With the short time frame available until Generation IV RPVs commence construction, this creates difficulty with regard to its assessment for service. A potential concern regarding the application of Grade 4N is that it may have increased susceptibility to irradiation embrittlements. This is due to the fact that Ni has increased elemental sensitivity to irradiation with increasing Cu content. However, research has hypothesised that if the Cu content is maintained at a low level, irradiation will not occur [28-30]. Despite this Grade 4 is the only viable material currently available to extend the lifetime of nuclear power plants to 60+ years [28].

With the desire for increasing plant capacity, the design and manufacture of RPVs have evolved with a number of geometrical constraints. In the 1950s RPVs were constructed from a number of rolled plates welded together to fabricate a large cylinder. However newer manufacturing techniques allow the RPV to be formed from monoblock-forgings eliminating the need for welds. These weld regions were significantly weaker and thus the main areas in which cracks were likely to initiate [33]. As such modern manufacturing technique allows increased integrity and more efficient processing of the forged RPV. The size and dimensions of RPVs varies according to the power capacity requirements of the plant with the core being dependent on total power and fuel life. As power capacity demand has increased the dimensions of the RPVs has increased. Consequently, the thickness of the pressure vessel wall must be enhanced in order to maintain the required strength [3].

The European Nuclear Society cites that the standard dimensions for

RPVs within nuclear plants are 5 m in diameter, 12 m in height with a weight of approximately 530 tonnes. The vessel itself experiences service conditions of 17.5 MPa of pressure and 350°C [34].

With significant evolution of design and materials used in RPVs, the fabrication process of this component is crucial in order to optimise the microstructural evolution. Thus, this work will focus on an extensive investigation of Grade 4N in order to develop a deeper understanding of the material both from a microstructural and mechanical perspective under varying service conditions. The aim is to ascertain whether Grade 4N steel is capable of meeting the nuclear industry's requirements in order that it may be brought in service. Particular focus is given in this report to the austenite grain growth of SA508 Grade 4N.

2.4   Fabrication of a reactor pressure vessel

Reliability and performance are crucial when commissioning the large forgings necessary in the manufacture of RPVs [3]. Casting, refining and forging technology have all been optimized in recent decades: the double degassing method is employed to reduce impurities with the multi-pouring method allowing larger ingots to be formed [35]. Vacuum induction melting and electroslag re-melting furnaces aid construction of high performance and large scale RPVs. Both these techniques refine the microstructure, remove impurities and reduce macrosegregation. A second driver in the manufacture of larger forgings is the ability to integrate components minimizing the number of welds reducing the likelihood of stress corrosion cracking and other weld-related issues [35].

RPV fabrication consists of a series of processes. The composition of the scrap steel used in the electric arc re-melting process is of significant importance to the meeting of compositional requirements. This is to avoid, as far as possible, detrimental elements, such as phosphorus, copper and bismuth, which may lead to embrittlement. The optimisation of steel-making practises and manufacturing routes has meant that the scrap metal used has increased purity compared to previous years resulting in significant reduction in impurities [3, 36].

The initial stage in RPV manufacture is the casting of an ingot of the specified chemistry and mass. RPV forgings can be composed of various grades of SA508 steel to meet the in service property requirements. Scrap steel is placed in an electric arc melter until it reaches the required chemistry and weight. The re-melted steel is then vacuum degassed upon pouring into metallic moulds producing a high quality ingot with minimal gases such as hydrogen, oxygen and nitrogen [3, 37]. The vacuum degassing stage is critical to the formation of a high quality ingot especially for thick-walled steel components; in order to gain an optimised balance between strength and toughness minimising heterogeneities.

The ingot then undergoes several forging passes allowing the manufacturer to select the desired geometry. RPVs can be produced to various dimensions and shapes with cylindrical components being the more favoured design; these cylindrical designs can be [37]:

1. open-ended cylindrical vessel: manufactured by punching a hole through the centre of a solid ingot after the removal of the top and bottom.

16

2. Blind-ended vessel: a similar method to Open-ended but where the ingot which has had the top and bottom discarded is blind-end bored.

3. Open-ended vessel: produces a hollow ingot.

The design will influence the overall processing, testing and properties.

The forging operations occur above the temperature at which ferrite completes its transformation to austenite, Ac_3, thus they occur while the steel is fully austenitic [3]. The forging stage allows the refinement of the as-cast microstructure via dynamic recrystallization leading to improved mechanical properties. Sufficient plastic work at this stage allows the break up of inclusion clusters, and minimisation of the porosity in the as-cast ingot. The forging steps for a cylindrical RPV comprise: [36-38]

1— cogging- forms the ingot into a plain sided cylinder which can then be worked perpendicularly allowing the central region to be consolidated breaking up the columnar microstructure closing the pores formed due to solidification shrinkage. Kakimoto *et al.* [39] discovered, utilising finite element simulations, that in order to consolidate the pores within the central region it is necessary to employ a reduction ratio of 75 % [39].

2— Upsetting- this forging mechanism allows dynamic recrystallization to occur leading to a reduction in the length of the ingot and an increase in cross section forming a disc.

3— Trepanning- this stage is crucial in the removal of the central region of the forged ingot in order to improve the homogeneity of the microstructure. The ingot is cored in order that a mandrel can be utilised for the drawing operation.

4— Drawing- the bore is increased allowing the forging to be drawn to the desired length. As the forging length is increased the wall thickness reduces. The forging is then rotated on the mandrel bar.

5— Becking- this optimises the wall thickness with work being carried out equally in both longitudinal and circumferential directions.

The large dimensions of the ingots used in the fabrication of RPVs creates issues in that upon casting macroscopic segregation will inevitably occur. The biggest effect is in the centre of the ingot due to a slower cooling rate than at the outside edge. Thus by removing the centre section the heavy inclusions and macrosegregation are eliminated. Hollow ingot technology was developed in the 1980s as an alternative to solid ingots allowing shorter solidification times reducing the macrosegregation compared to the solid ingot [36-38].

Earlier smaller pressure vessel designs were able to provide the desired strength and toughness allowing ease of manufacture. However today's larger pressure vessels now have a more stringent target in order to achieve the required properties. The manufacturer is required to ensure that there is minimal variation in mechanical properties with heterogeneities being reduced by refining passes prior to quenching [37].

To control the heterogeneities throughout processing it is necessary to simulate the techniques in order to optimize the manufacturing routes. Ingot size, compositional selection, weight and pouring temperature

are all parameters that directly affect the segregation, inclusions and porosity [37].

Heat treatment is the next fundamental phase in the manufacturing route with two principal aims, firstly to gain the desired properties and secondly, to refine the microstructure. This phase is performed in two heat treatment stages: "primary" and "quality" [3,36].

The first heat treatment stage is carried out after forging in order to relax the induced strain that was caused by the hot working of the component; allowing the refining of the microstructure. Ultrasonic testing is carried out on the component in order to confirm that it meets the required structural integrity [35,37].

Cogswell describes the overall manufacturing process of RPVs in considerable detail as illustrated in Figure 2.4 [36]. Air cooling of the component with a hold at 500°C allows for completion of the austenite to ferrite phase transformation followed by a second hold at 250°C in order to avoid the probability of hydrogen cracking due to catastrophic through thickness failure. The component is held at 600°C allowing for the diffusion of hydrogen to occur the time for this to occur is dependent on the thickness of the component. Homogenisation then occurs at 900°C, allowing for the dissolution of the second phase, followed by air cooling and finally a tempering stage between 600°C - 650°C to soften the forging ready for machining [36].

Figure 2.4: Forming process for the RPV [36].
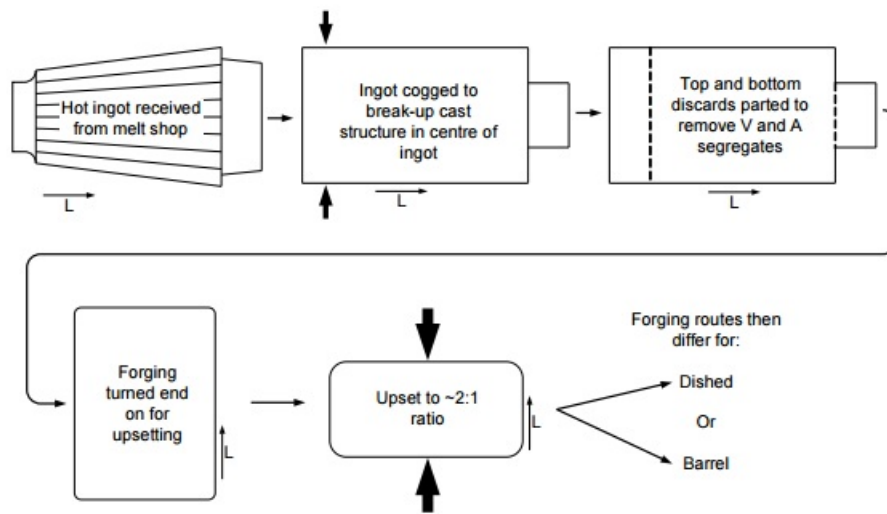
Following primary heat treatment the forging is machined to a net shape before undergoing a final quality heat treatment to obtain the desired properties. The RPV is then the correct geometry facilitating non-destructive inspection, typically ultrasonic, to confirm it has the desired structural integrity [36]. Section 2.6 describes the heat treatment in more detail.

Figure 2.5: "Primary heat treatment" [36].
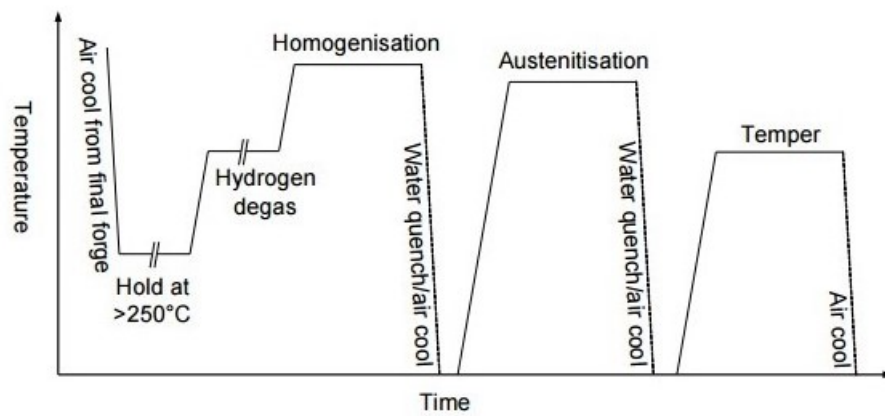
2.5 Quality heat treatment

Following forging heat treatment is undertaken for two principal reasons; firstly, to gain the properties desired and secondly, to refine the microstructure. The component properties are influenced by the microstructure, which is based on the heat treatment, are a function of the thickness and chemical composition. Key properties include homogeneity, minimisation of harmful defects, increased fracture toughness and resistance to embrittlement. The variance in heating rate, cooling rate, through-thickness and hold time must all be considered prior to selecting the appropriate heat treatment process [40].

As outlined in Section 2.4, primary heat treatment is undertaken in order to relax the induced strain before refining the coarse microstructure to provide transparency for non-destructive inspection. This primary heat treatment allows the refinement of the coarse grained microstructure for increased toughness [40, 41].

The second stage heat treatment composed of austenitisation followed by quenching and is undertaken once the component is near net shape as the reduced wall thickness and weight provides increased quenching efficiency as a result of the decrease in thermal mass and shorter path for heat removal (Figure 2.6). The initial austenisation stage allows for the dissolution of precipitates and secondary phases with the second optional austentisation stage being utilised to improve the through thickness properties of the component [36].

The austenitising temperature is based on the ASTM code. For Grade 4N Class 1 and 3 this is specified as a minimum of 840°C and a max-

imum of 895°C. The Grade 3 austenitisation temperatures are unspecified by the ASTM code and based on the manufacturers knowledge. The temperature is chosen so that the majority of carbides within the steel are dissolved. The quenching stage is carried out using a liquid by spraying or immersion. For tempering of SA508 Grade 4 the ASTM code specifies that for the minimum tempering temperatures are: 595°C for Classes 1 and 2, and 605°C for Class 3. After tempering the components are welded together to form the finished RPV and are subjected to post-weld heat treatment (PWHT) [3, 30].

Heat treatment and composition are critical to achieving the optimum balance between strength and toughness; of the two, heat treatment is the easier to modify in order to optimise the properties. The size of the component determines the austenitisation time sufficient to achieve a homogenous microstructure [3, 30].

Lee *et al.* [27] found that by applying rapid cooling following austenitisation resulted in an increase in tempered martensite fraction leading to increased refinement of carbides. However due to the size of the component rapid cooling is difficult to control in RPVs. PWHT allows the reduction of residual stresses in the weld region by heating. Grade 3 is tempered at 660°C with a following PWHT stages at 610°C. Many researchers have applied these conditions to Grade 4N without considering the the difference in composition. Lee *et al.* [27] investigated Grade 4N to seek to determine the optimum tempering and PWHT conditions. Four different heat treatments were explored with the as-tempered state at 630°C leading to an under-tempered region being partially formed due to the low tempering temperature, producing a non-uniform matrix resulting in a large scatter of properties. It was discovered that

on increasing the PWHT temperature that the ductile-brittle transition temperature (DBTT) increased due to the increased formation of coarse carbides which controlled cleavage initiation. Further research into heat treatments for Grade 4N steels needs to be undertaken in order to fully evaluate the most effective heat treatments [27].

An investigation of 15 concept alloys of Grade 4N undertaken by Lee *et al.* led to the observation that Cr-carbides, of M_7C_3 and $M_{23}C_6$, precipitated in these candidate alloys [42]. This is in comparison to the Grade 3 steels which due to their lower Cr content form coarse M_3C carbides. Im *et al.* investigated the effect of carbon content with regard to DBTT and Upper Shelf Energy (USE) [43]. It was found that with decreasing carbon content a lower DBTT and increased USE occurred. The lowering of the DBTT due to the decreased carbon content confers increased cleavage fracture stress. With a lower carbon content the likelihood of the formation of cementite precipitates is reduced [43]. These cementite inter-lath precipitates, which are known sites for the initiation of fracture, are reduced in size with the decrease in carbon content leading to increase in cleavage fracture stress [42, 43].

Austenitisation and the resultant microstructure are discussed further in Section 2.5.1.

Figure 2.6: Quality heat treatment [36].
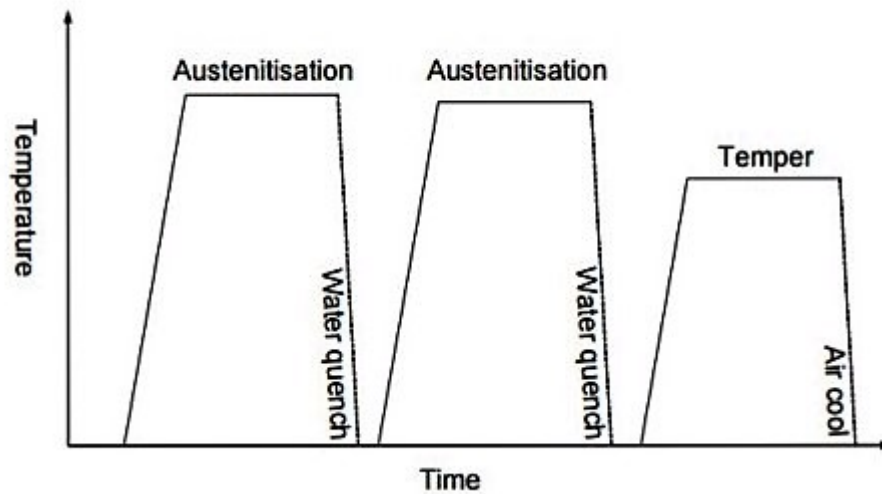
2.5.1 Austenitising

Grain size is critical to the mechanical properties of the final component. The control of the austenite grain growth and size allows the refinement of the bainite laths in both length and thickness, which are limited by the austenite grain boundaries [44]. The two main methods used to control the austenite grain size are the austenitisation process and the pinning of boundaries by fine precipitates. The austenite grain size directly affects the hardenability of the component. However there is little significant literature on the austenitising process for Grade 4N [44].

Sellars *et al.* modelled the austenite grain growth with the assumption that the rate of change of grain growth is dependent on the surface per unit volume. In certain cases the initial grain size is significantly smaller than the grain size after coarsening and thus its influence is neglected [45]. This classical model makes assumptions that disregard the fact that the initial grain size is a function of temperature due to the austenite grains being formed by nucleation and growth.

25

Vanherpe *et al.* [46] discussed second-phase particle pinning at grain boundaries based on fundamental research by Zener. These particles restrict the movement of the grain boundaries, inhibiting their growth and limiting the grain size of the final microstructure. If the particles were to grow beyond a critical size they agglomerate, grow in size and become coarse and few in number causing the final component to be of poor quality [43, 44, 46]. An example of such precipitates are AlN.

Overall there is a significant lack of literature on the austenitisation process and cooling rates on Grade 4N steels. Thus one of the aims of this research project is to provide further evidence as to how the austenitisation temperature affects austenite grain size.

2.5.1.1 Modelling of austenite grain growth

Modelling of the grain growth of the austenite is of paramount importance in refining the properties of the final RPV.

Initial models for grain growth were established by Beck *et al.* utilising equation 2.3 [45]:

$$D^n - D_0^n = A \exp\left(\frac{-Q}{RT}\right) t \tag{2.3}$$

where D is the grain size, D_0 is the initial grain size, t the holding time, A is a constant, Q is activation energy, R and T have their usual scientific meaning.

This equation provided the basis for many models describing austenitic grain growth. Wang *et al.* [47] produced a new model accounting for

the second phase particle pinning and more recently Lee *et al.* defined a simplified model, Equation 2.4 [27, 44, 47]:

$$D = A \exp\left(\frac{-Q}{RT}\right)t \qquad (2.4)$$

This new model negates the initial grain size as it is assumed to be significantly smaller compared to the final size.

It is essential that when modelling grain growth a quantitative analytical description of the structures can be explained. This means that it is critical to compare the theoretical predictions and experimental results. An estimate of the grain boundary area per unit volume S_v is utilised as a tool for further analysis in order to correlate grain boundary interactions with properties. The grain boundary area per unit volume is able to be calculated from experimental measurements of mean lineal grain intercept [46].

Pous-Romero *et al.* [3] modelled the grain growth for continuous heating between A_c3 and the desired temperature for heat treatment utilising the following equation:

$$-DD_{LIM} - (D_{LIM}{}^2)\ln\left(1 - \frac{D}{D_{LIM}}\right) + D_{Ac3}D_{LIM} + (D_{LIM}{}^2)\ln\left(1 - \frac{D_{Ac3}}{D_{LIM}}\right)$$
$$= A\exp\left(\frac{-Q}{RT}\right)t + \frac{A}{\alpha}\int_{Ac3}^{A}\exp\left(\frac{-Q}{RT}\right)dT$$

$$(2.5)$$

where D_{LIM} is the limiting grain size, D_{Ac3} is the grain size at A_c3 and α is the heating rate. This method accurately predicted the grain growth for Grade 3 steel which undergoes pinning due to AlN precipitates [3].

It is found with the majority of models that grain growth can be concluded as being driven by the minimisation of grain boundary area per unit volume and as such a decrease in free energy. However these classical models are specific to certain steels and may require modification in relation to SA508 Grade 4N.

2.6 Thermal grooving

Thermal grooving, also known as Thermal etching, is a technique that was first discussed in a paper by Mullins [51] entitled *Theory of Thermal Grooving*. It is utilised to reveal grain boundaries for characterisation. The method is based on the transfer of matter away from grain boundaries upon heating. During heating the intersection of the vertical grain boundary and polished surface meet with a known angle at a triple point leading to a local equilibrium. Surface tension causes grooves to form on the polished surface. It is accepted throughout literature that the surface grooves which are formed by stationary grain boundaries replicate the grain structure of the bulk material [3, 44,49-51].

Mullins [51] research showed that grooves may pin boundaries preventing migration under the conditions of slow grown growth [50,51]. This technique will be utilised to investigate the prior austenite grain size of Grade 4N specimens.

2.7 Microstructure and properties

The main difference between the Grade 3 material currently used and the new Grade 4N material is the higher Ni and Cr contents and reduced Mn content in the latter (Table 2.1). The lack of long-term in service data for Grade 4 means that further research needs to be undertaken to gain knowledge on the effect of service conditions on the microstructure [28].

Literature regarding the microstructural characterisations of Grade 4 has shown diverse conclusions. Investigations by Lee *et al.* found that

Grade 3 has a bainite microstructure with coarse cementite particles. Conversely Grade 4 has a tempered martensite microstructure with minimal carbides in a refined state. However fine precipitates of M_7C_3 and $M_{23}C_6$ are formed in the Grade 4 microstructure following tempering. The conclusion that the Grade 4 microstructure was martensitic is, however, in contrast to research undertaken by Burke *et al.* and Park *et al.* [28, 52-53]. As such the resultant microstructure is significantly dependent upon the cooling rate and heat treatment.

It is difficult to identify whether the phase fractions in Grade 4 are lower bainite or tempered martensite due to their similar lath structures. Park *et al.* [54] employed scanning electron microscopy images and electron back-scattered diffraction to determine the phase fractions [54]. The increase Ni content reduced the amount of bainite leading to a decrease in effective grain size due to the remaining austenite transforming into martensite. This increased martensite fraction provides increased strength and fracture toughness. Park *et al.* further investigated alloys with varying Ni content (Table 2.3) which resulted in varying microstructure. Alloy A with the lowest Ni content was found to have coarse bainitic laths with martensite packets within the prior austenite grain boundary. The packets of martensite were smaller than in Alloy B with a lower bainitic fraction. Alloy B had a similar composition to the alloy being investigated in this project [54].

	C	Mn	Ni	Cr	Mo	Fe
A	0.21	0.33	2.66	1.81	0.53	Bal.
B	0.19	0.30	3.63	1.87	0.54	Bal.
C	0.21	0.32	4.82	1.83	0.53	Bal.

Table 2.3: Chemical composition of steel (wt%) from Park *et al.* [54].

Lee *et al.* found that yield strength and impact toughness were im-

proved by an increase in the fraction of tempered martensite at room temperature [27]. A new heat treatment process, Inter-critical Heat Treatment (IHT), for Grade 3 has been developed which results in increased fractions of martensite and enhances strength and toughness. IHT is undertaken following quenching and prior to tempering. This process has been known to increase the ductility and USE with a decrease in the DBTT [55]. This process produces a composite microstructure composed of tempered martensite and double tempered bainite for Grade 3 SA508 leading to a finer and more homogeneous microstructure. Ahn *et al.* [55] found that the increased toughness was due to the increased inter-carbide distances induced by IHT.

Xia *et al.* [52] investigated the use of IHT in the manufacturing process of Grade 4. Their findings accorded with those of Lee *et al.* [27] in that they determined that the microstructure following quenching and tempering is lath martensite and plate like bainite with some precipitate. The martensite is formed from the parent austenite during the cooling stage, thus cooling is crucial to the final microstructure [52].

The coarse carbides are dissolved during heating with the austenite phase forming along the grain and lath boundaries in which the carbon content increases. Upon cooling this region transforms to martensite in sufficient quantities via the two step process of quenching in air and tempering. The fine precipitates were concluded to be of type M_7C_3 and $M_{23}C_6$ and formed at the interface between martensite laths [52].

A comparison of Grade 3 and Grade 4 found that the change in chemical composition resulted in enhanced mechanical properties with the area below the stress-strain curve being greatest for the Grade 4 vari-

ant. Xia *et al.* [52] showed that the elongation after fracture was also greater for Grade 4 had an increase of 10 % compared to Grade 3. This was attributed to the lath martensite. Microstructure has a significant effect on the properties of the material.

Table 2.4: Mechanical Properties SA508 Grades [30].

Identity	Grade 1 / 1a	Grades 2 Class 1 / 3 Class 1	Grades 2 Class 2 / 3 Class 2	Grades 4N Class 1 / 5 Class 1	Grades 4N Class 2 / 5 Class 2	Grades 4N Class 2 / 5 Class 2
Tensile Strength [MPa]	485-655	550-725	620-795	725-895	795-965	620-795
Yield Strength [0.2% offset]	250	345	450	585	690	485
Elongation min %	20	18	16	18	16	20
Reduction of area, min. %	38	38	35	45	45	48

2.7.1 Through-thickness properties

As RPVs are large components with thick walls it can be difficult to ensure that the microstructure is homogenous. The cooling rate following austenitisation varies with depth leading to variations in microstructure. The microstructure of the component therefore depends on the location within the wall. Slow cooled regions may not achieve the desired properties. It is therefore critical that the entire manufacturing process and specifically the quenching is modelled in order to determine the slowest cooling region [3, 31, 44].

Little literature exists regarding the hardenability of Grade 4N. However research relating to the hardenability of Grade 3 identified that the through-thickness mechanical properties were symmetrical about the midpoint of the component wall. Pous-Romero *et al.* found that the austenite grain size has an influence on the hardenability of Grade 3 steels [3, 44].

Overall it can be concluded that microstructural properties are location-dependent from the surface of the component. The cooling rate from the austenitisation temperature is critical to the homogenous distribution of properties. It has also been suggested that the magnitude of variations in these properties is dependent on the thickness of the RPV; with the thicker RPVs having increased heterogeneities [36].

2.8 Strengthening Mechanisms

Strengthening mechanisms are utilised in order to gain the desired mechanical properties for industry. Different mechanisms can be implemented to gain strength in the material: grain strengtheing, solute atom additions and fine particle additions. These strengthening mechanisms are discussed below.

2.8.1 Grain boundary strengthening

Through the use of experimental research significant evidence for the mechanical strengthening of grain boundaries has been found. Notably it was discovered that a grain boundary has minimal inherent strength and that mutual interference with slip within the grains is the main mode of strengthening. Two scientists Hall and Petch individual proposed a relationship between describes the relationship between yield stress t and grain size d of a polycrystalline material [56,57]:

$$\tau = \tau_0 + kd^{-1/2},\tag{2.6}$$

where τ_0 is the friction stress considered needed to move individual dislocations, and k is a constant (often referred to as the Hall-Petch slope and is material dependent).

This equation is able to illustrate the grain size dependence with regard to resistance to dislocation movement and fatigue strength. This model was based on grain boundaries acting as pinning barriers for the movement of dislocations. However Hall-Petch equation was found to be somewhat general for many cases. Significantly if the above equa-

tion was based on large dislocation pile ups of at least 50 dislocations and thus would not be suitable for small grain size strength predictions [56,57].

2.8.2   Solid solution strengthening

Another mechanism utilised is the addition of solute atoms. These allow the formation of an alloy that is stronger than the metal in pure form. There are two classifications of solid solutions. If the size of the solute and solvent atoms are similar then the solute will occupy lattice points this is known as a substitutional solid solution. However if the solute atom is significantly smaller then it occupies the interstitial positions in the lattice of the solvent. Carbon and nitrogen fall into this category and form interstitial solid solutions [56,57].

2.8.2.1   Substitutional solid solution

Substitutional solid solution strengthening was first developed through work undertaken by Hume and Rothery. A wide range of metallic elements may be used to form substitutional solid solutions. If the difference in lattice parameter between the solvent and solute is less than 15% then substitutional solid solution is favourable. Where there is a lack of strong chemical affinity metals tend to form solid solutions. These metallic elements can cause a significant variance in strength. Hume-Rothery size effect details that the strengthening by substitutional solute atoms is dependent on the difference in atomic size of the solute and that of the iron. It is usual for these atoms to form spherical distortion with a relative strengthening of modulus of rigidity/10 [56-61].

2.8.2.2 Interstitial solid solution

Solid solution strengthening mechanism can be caused by substituting atoms for iron. This leads to expansions or contractions in the lattice. These misfitting substitute atoms cause strains fields leading to the inhibiting of dislocation movement this is due to the production of non-spherical distortions. In austenite it is found that the interstitial site is a regular octahedron and behaves as a substitutional solute causing isotropic strains to occur. This means that the site is surrounded by strains that only interact with the hydrostatic strain fields of the dislocations. As such carbon and nitrogen have less effect on the strengthening of austenite due to their regular octahedron nature[56,60-61].

2.8.3 Precipitation strengthening

This strengthening mechanism occurs when precipitates are formed inside the grains of an alloy. These precipitates inhibit dislocation movement however the extent at which they cause this inhibition is based on a number of factors. These include the strength, size, shape and distribution of the precipitates. Notably when dislocations encounter a precipitate there are a number of ways in which it is able to continue to travel: cut through the precipitate or loop around it [56,57,62]

2.8.3.1 Cutting

Cutting occurs when a dislocation shears a precipitate leading to the dislocation experiencing a subsequent resistance to motion. This resistance can be caused by an increase in surface energy which is due to a ledge forming on the precipitate after cutting. However this increase in surface area to volume ratio of the precipitates can leads to their dis-

solution due to the destabilised nature of the now smaller precipitates [56,57].

2.8.3.2 Looping

If the stress for cutting a precipitate are excessively high then looping will occur. As a dislocation approaches a precipitate it loops around it. This is sometimes known as Orowan looping [56,62].

2.9 Future

RPVs operate under extreme conditions at high temperatures, stresses, corrosive environments and with neutron irradiation. These conditions mean that the structural materials chosen must have exceptional properties. Under standard operating conditions most PWR reactors function at between 270°C and 330°C with a high pressure of 15 MPa. Grade 4N has suitable creep resistance, strength and toughness properties at the start of life however little research has been undertaken into the irradiation effects [28].

Due to the nature of these critical components strict regulations are imposed on industry to minimise the probabilities of failure. Safety margins are employed that ensure the materials utilised have properties which are significantly superior than the maximum service requirements. As there are currently few operational data available for Grade 4N, much of the knowledge of this material is based on small scale laboratory research.

2.9.1 Irradiation embrittlement

With increased Ni content there is heightened concern that SA508 Grade 4N will be more susceptible to irradiation embrittlement, which is a process whereby the number density of point defects increases and induces phase transformations and void formation. Chemical composition is a key factor in the sensitivity of a steel to irradiation embrittlement. Due to the complicated operating conditions and material factors there is no standardised theory with regard to the prediction and location of these effects. In order to develop an understanding of irradiation embrittlement small specimens of the RPV material are placed in reactors in service and removed for investigation over time [3, 28]. In short, irradiation embrittlement increases the hardness and decreases the ductility leading to a reduction in toughness.

Burke *et al.* [53] examined the irradiation damage of SA508 concluding that the Ni content was not the controlling factor, rather the Mn content. The mechanical properties of the steel were found to change upon irradiation due to precipitation of clusters containing 6% Cu [51-53].

Lee *et al.* undertook experiments investigating the irradiation effects on 12 alloys with varying compositions (Figure 2.7). The irradiation hardening effect was found to be similar for Alloy A (Grade 3) and Alloy B (Grade 4N). The other alloys tested had both increased Ni and Mn content and showed certain extreme property changes. These findings confirmed previous investigations by several research groups. Lee *et al.* established that with an increase in Ni and Mn content the irradiation hardening effect increased however as the ASTM code limits Mn content for Grade 4N to 0.4%; the deleterious irradiation embrittlement is unlikely to be of a serious concern (Figure 2.8). Ultimately further in-

depth investigation of Grade 4N needs to be undertaken to characterise the irradiation behaviour of this novel material [28].

Figure 2.7: Adapted from B-S Lee Hardness (Hv) of alloys comparison before and after irradiation [28].
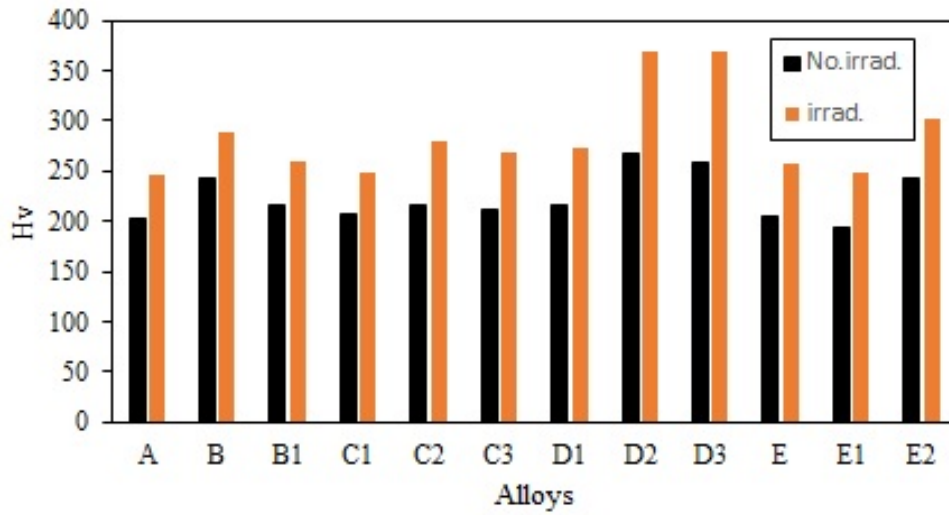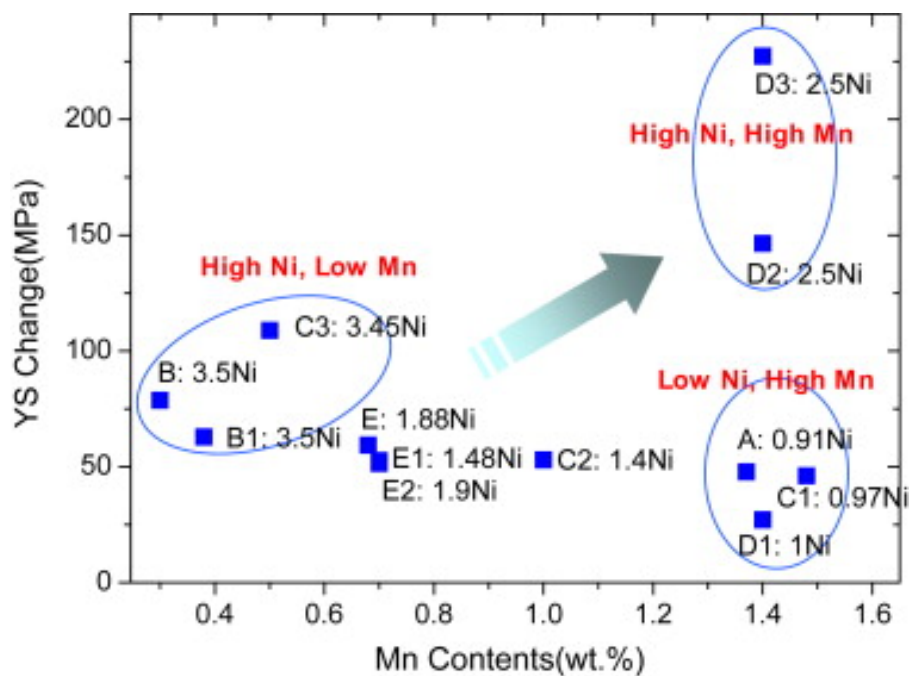
Figure 2.8: Effects of Mn and Ni with regard to the yield strength (YS) post irradiation [28].

2.9.2 Importance of SA508 Grade 4N

With increasing demand for nuclear power plants with a longer life-time and increased capacity a new material is required to meet these requirements. As the RPV can be the critical lifelimiting component in a fission reactor any new material must demonstrate increased durability, toughness and strength. SA508 Grade 4N is a suitable candidate material with enhanced mechanical properties compared to SA508 Grade 3 currently in use. However as outlined there is little experimental data from in service applications of this candidate material.

This research project will expand upon studies which have been undertaken drawing on acknowledged techniques. Thus it is the aim of this research to provide an in depth investigation into the microstructural behaviour of Grade 4N under varying conditions with specific focus on the austenite grain size.

3 — Experimental Methods

3.1 As-received material

The steel being investigated is SA508 Grade 4 (Table 3.1) from an unspecified part of the outer region of a 100 tonne forged nuclear pressure vessel supplied by Rolls Royce Nuclear. The composition of the supplied alloy is displayed in Table 3.1.

The material was supplied in a block, 240 mm x 210 mm x 155 mm, in a quenched and tempered condition. As-received material was then machined for experimental analysis.

Table 3.1: Composition of Grade 4N Steel wt%

Identity	C	Si	Mn	P	S	Cr	Mo	Ni	Al	Co
	0.207	0.102	0.349	0.005	0.001	1.866	0.502	3.867	0.004	0.016
	Cu	Nb	Ti	V	W	Pb	Sn	Ca	B	N
	0.023	0.004	0.01	0.048	0.008	0.003	0.002	0.001	0.0002	0.0065

3.2   Metallographic preparation

A 2 cm thick section of the as-received material cut transverse to the forging direction was ground and polished prior to macroetching using 5% nitric acid in methanol. Cylindrical samples were machined from the as-received material with the following dimensions (Table 3.2). It should be noted that samples of varying dimensions were produced due to the range of holding times and equipment availability.

In preparation for thermal etching samples were then hot-mounted in bakelite, at 150° C and 2 bar pressure. The samples were then ground utilising 240-grit silicon carbide paper up to 4000-grit silicon carbide paper revealing a flat surface parallel to the longitudinal axis. Samples were next polished using first 6 μm and then a 1 μm diamond paste with water based lubricant. The samples were then broken out of the bakelite prior to thermal etching.

Table 3.2: Dimensions of the dilatometry samples for the different machines

Machine	Diameter/ mm	Length/ mm
Thermecmastor-Z	8	12
DIL805	4	10
Furnace	8	12

3.3   Optical micrography

Optical microscopy was utilised using Olympus BH microscope with a Leica DFC295 camera.

3.4   Scanning Electron Microscopy

Scanning electron microscopy was carried out utilising the Phenom ProX SEM in order to analyse in more detail the presence of martensite lathes which were shown in the optical micrographs.

3.4.1   Thermal etching

Thermal grooving was utilised to reveal austenite grain boundaries. The pre-polished samples were heated to form grooves due to the balancing of surface tension forces [51].

3.4.2   Grain size measurements

The linear intercept method was utilised in order to calculate the grain size for the varying austenitising temperature and hold times. A total of 100 linear intercept lines were utilised with the average value being recorded as the linear intercept.

A 95% confidence interval was calculated based on Pous Romero *et al.*'s method (Equation 3.1) [3,63].

$$95\%CI = 1.96 \times \frac{\sigma_x}{\sqrt{N_{LI}}} \tag{3.1}$$

where σ_x is the standard deviation of the values and N_{LI} the number of linear intercept lines. This value was then utilised to obtain the error based on the percent relative accuracy (Equation 3.2).

$$\%RA = \frac{95\%CI}{\overline{LI}} \times 100 \qquad (3.2)$$

Where $(\overline{LI})$ is the average linear intercept.

ImageJ was utilised to analyse the grain size distribution [64]. The maximum error was found utilising the following Equation 3.3:

$$\text{Error μm} = \overline{LI}(\text{μm}) \times \frac{RA\%}{100} \qquad (3.3)$$

Pous Romero *et al.'* [3] predictive model was then utilised to see whether the grain size for SA508 4N could be accurately predicted . Significantly this model is based on steels, such as Grade 3, which are known to contain grain boundary pinning AlN precipitates. A fortran code was utilised based on the following Equation 3.4:

$$-DD_{LIM} - (D_{LIM}{}^2)\ln\left(1 - \frac{D}{D_{LIM}}\right) + D_{Ac3}D_{LIM} + (D_{LIM}{}^2)\ln\left(1 - \frac{D_{Ac3}}{D_{LIM}}\right)$$
$$= A\exp\left(\frac{-Q}{RT}\right)t + \frac{A}{\alpha}\int_{Ac3}^{A}\exp\left(\frac{-Q}{RT}\right)dT$$
$$(3.4)$$

where D_{LIM} is the limiting grain size, D_{A_c3} is the grain size at A_c3 and α is the heating rate and A is a known constant. This method was utilised to predicted the grain size for Grade 4N steel [3]. By inputting values which had been deduced experimentally the grain size D was able to be calculated and compared with the experimentally measured grain size

49

for a specific temperature and hold time.

3.5 Austenitisation

Samples prepared for thermal etching with the dimensions seen in Table 3.2 were utilised for investigating the effects of austenitising. These samples were heated under varying austenitising temperatures and hold times as seen in Table 3.3. Treatments up to 4 h, were carried out using the DIL805 with longer treatments up to 6 h in the furnace and all longer treatments being undertaken in the Thermecmastor thermomechanical simulator.

In both the DIL805 and Thermecmastor-Z the temperature, dilation and load are recorded as a function of time. The deviation of temperature is recorded by the S-type thermocouple as between $\pm 2°C$. The prepolished samples were heated under vacuum 5×10^{-3}Pa in order to mitigate against oxidation.

The heating and cooling rates utilised were $10°\text{C}\,s^{-1}$ and $30°\text{C}\,s^{-1}$ respectively. These were chosen in order to compare to previous experimental findings for Grade 3.

Samples held in the Elite Laboratory Chamber furnace were sealed in individual silica tubes with Argon gas and titanium sponge to prevent oxidation. Samples in both the DIL805 and Thermecmastor-Z were heated under vacuum and cooled also under vacuum.

Table 3.3: Varying austenitising conditions.

Machine	Temperature /°C	Hold time/ h
	840	0.5 1 2 3 4
	860	0.5 1 2 3 4
	880	0.5 1 2 3 4
DIL805	910	0.5 1 2 3 4
	940	0.5 1 2 3 4
	965	0.5 1 2 3 4
	990	0.5 1 2 3 4
	840	5 6
	860	5 6
	880	5 6
Furnace	910	5 6
	940	5 6
	965	5 6
	990	5 6
	840	7 8 9 10
	860	7 8 9 10
	880	7 8 9 10
Thermecmastor-Z	910	7 8 9 10
	940	7 8 9 10
	965	7 8 9 10
	990	7 8 9 10

3.6 Experimental hours

The section highlights the amount of experimental work that has been undertaken in excess of 460 hours of furnave time was carried out with over 100 assessments of varying heat treatments and over 10,000 grains were measured in total.

4 — Results

4.1 Austenite grain size measurements

A plot of mean linear intercept against austenitising hold times was produced based on previous experimental work by Pous-Romero *et al.* [3].

Based on current research it was uncertain as to whether SA508 4N obeys regular grain growth or whether it is limited ultimately by pinning particles whose nature has yet to be determined. The relationship between austentisation temperature, austenisation time and grain size in Grade 4N is shown in Figure 4.1, as determined by thermal etching. Austenitising temperatures are between $840°$C and $990°$C, and hold times between 30 min and 10 h with a heating rate of $10°$Cs^{-1}. As shown in the plot an increase in austenite grain size occurs over time at all temperatures, with the highest growth rates, and thus largest grain size, being observed at the higher austenitising temperatures. In all cases, as expected, there is an increase in grain size with increasing hold time. Detailed analysis of the data will be discussed in Section 5.

A comparison of how austenitisation temperature and hold times affects Grade 3 and Grade 4N is shown in Figure 4.2. Experimental findings by Pous Romero *et al.* [3] were plotted against the data for Grade

Figure 4.1: The grain size of Grade 4N with different holding times.
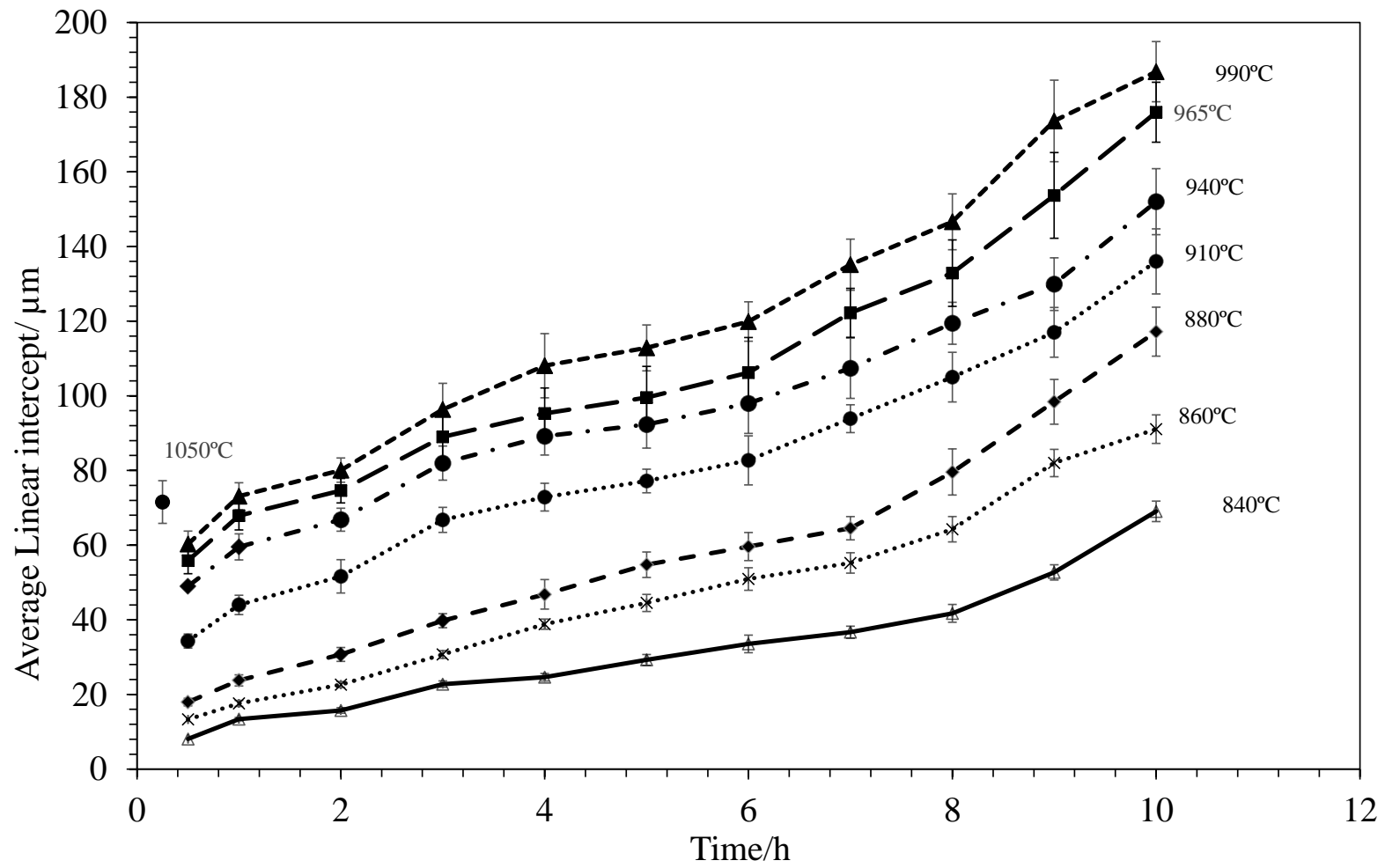
4N. Figure 4.2 clearly indicated that there is significant difference in the grain growth between the two alloys. The grain growth rate increase remains fairly constant and flat for Grade 3 at low temperatures, and there is a sudden acceleration after 910° C. In Grade 4N, however, the increase in grain size with temperature appears to continue as the temperature increases. Further discussion into this findings will be carried out within Section 5.

Figure 4.2: A graph of grain size of Grade 4N (black) and Grade 3 [3] with varying hold times.
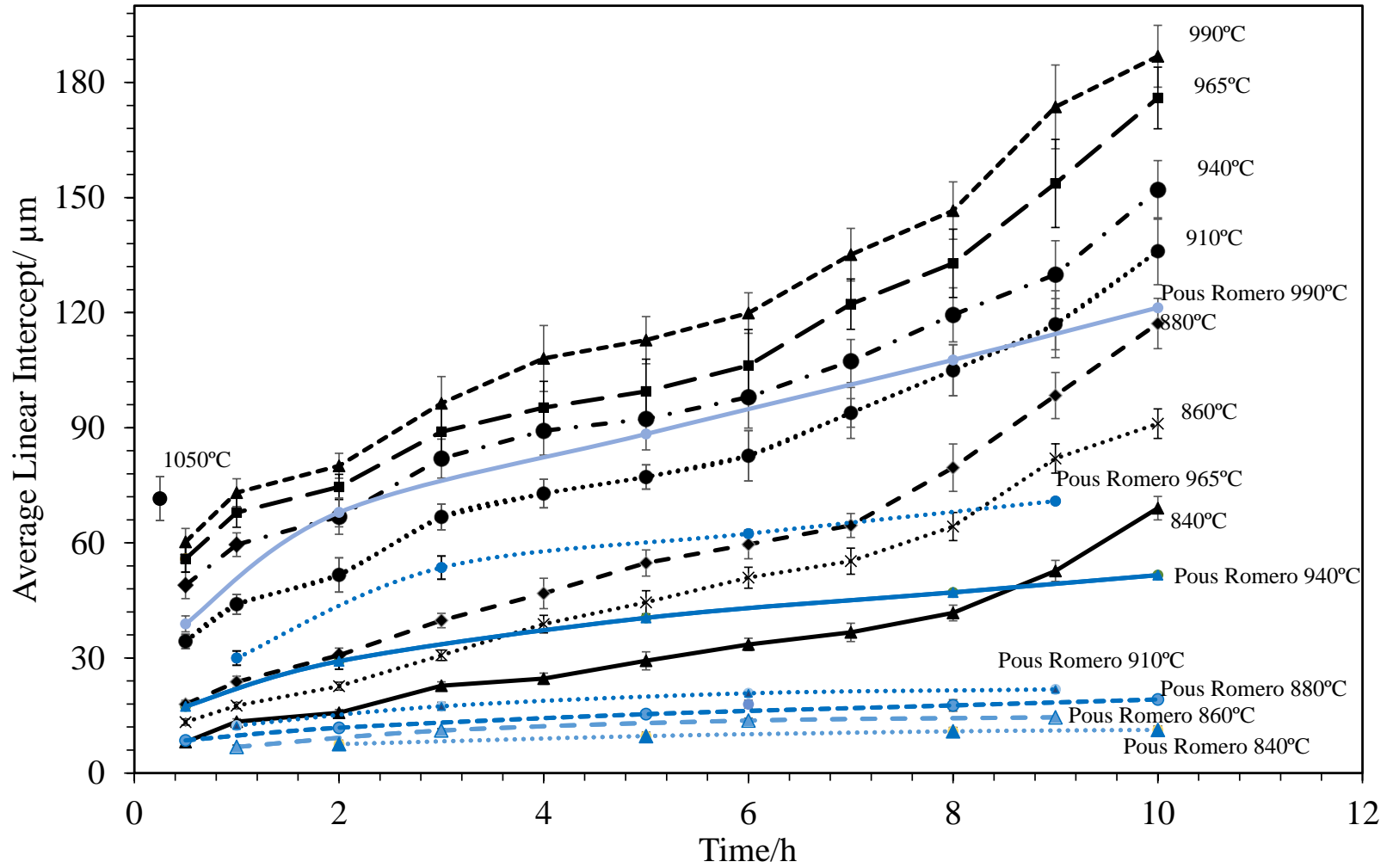
MT-DATA was used in order to calculate the wt% of the AlN precipitate for both the Grade 3 and Grade 4N alloys. Figure 4.3 shows that there is significantly more AlN precipitation predicted in the Grade 3 alloy than Grade 4N.

Figure 4.3: A graph varying wt% of AlN with time for Grade 3 (solid) and Grade 4N (dotted) [3].
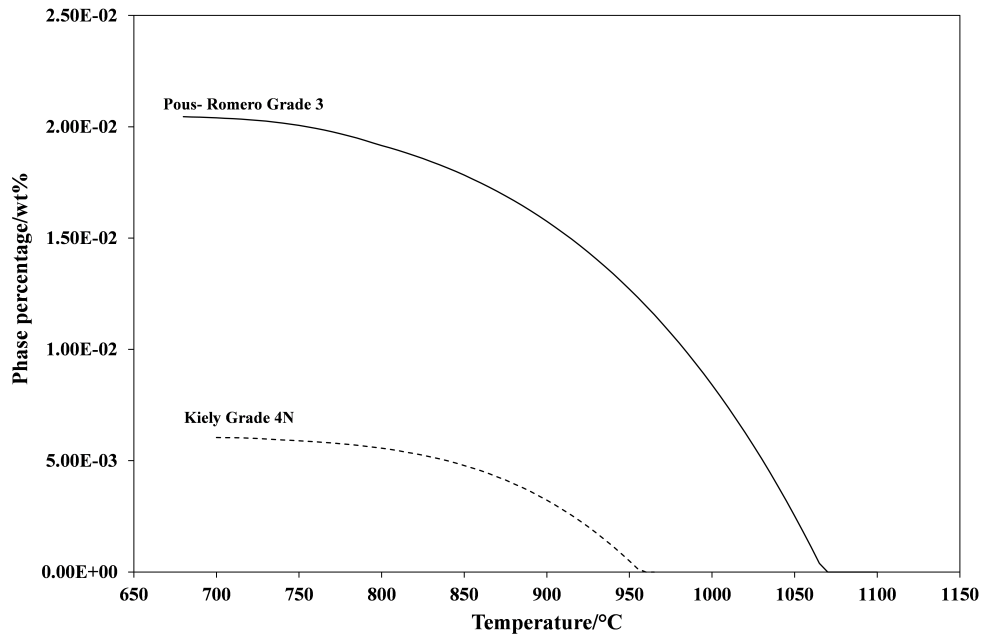
Utilising Fortran code, based on equation 3.4, [3] the grain size was able to be calculated for the composition of Grade 4N provided with the activation energy Q set at $190\,\mathrm{kJ\,mol^{-1}}$ based on previous experimental findings [3] and R has its usual meaning. This predicted grain size was then plotted against the experimentally measured size as illustrated in Figure 4.4. It is evident that the model was able to produce a good fit for the grain size of Grade 4N at lower temperatures however it lacked accuracy at higher temperatures. The benefits and limitations of this model as a predictive method are discussed within Section 5.

57

Figure 4.4: A comparison of the calculated grain size vs experimentally measured grain size of Grade 4N (Black) and Grade 3 (red).

y = 1.1008x
R² = 0.9714

Q = 190 kJ mol^{-1}
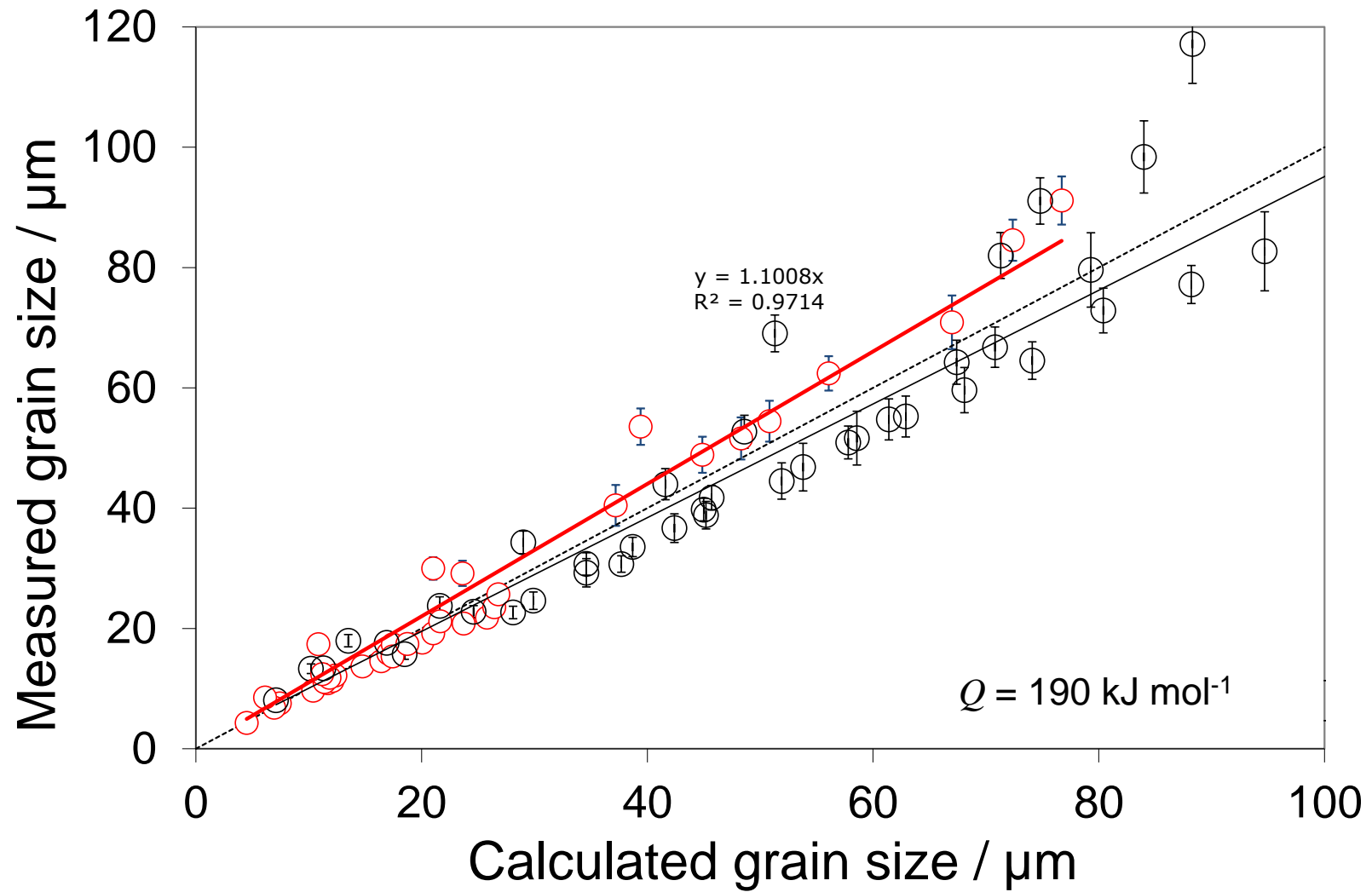
4.1.1 Comparison of austenite grain growth of Grade 4N and Grade 3

Pous-Romero *et al.*'s research showed that Grade 3 displays homogenous distribution of grain sizes at temperatures between 840℃ to 910℃ with the distribution changing to bimodal at higher temperatures (Figure 4.5). Figures 4.6 to 4.12 provide comparisons between Grade 4N (black) and Grade 3 (red) mean grain size with varying hold times for a specified temperature. At lower temperatures Grade 4N has significantly larger grain size disparity to Grade 3. Between 840° C and 910° C the grain size is at least double in size at the lower hold times increasing to up to seven times the size for longer holds. However above 940° C the disparity decreases somewhat and starts to converge at the higher temperature 990° C.
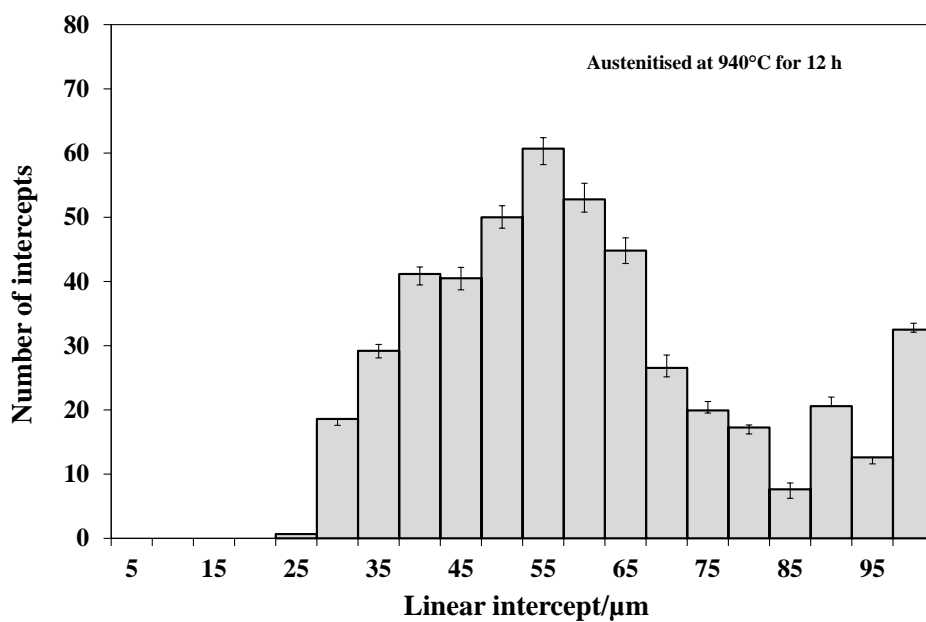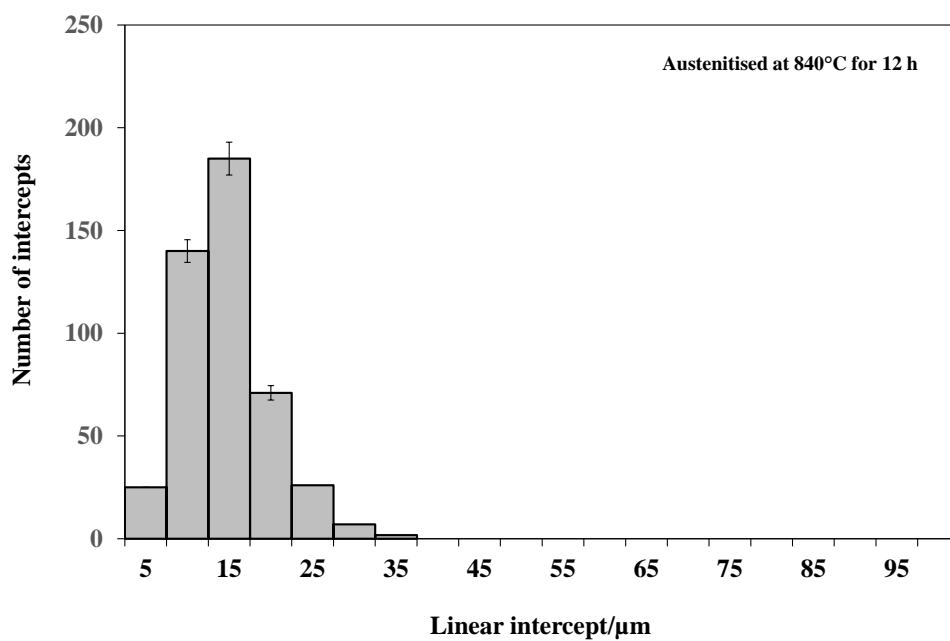
Figure 4.5: Linear intercept distribution for Grade 3 at 840°C and 940°C [3].
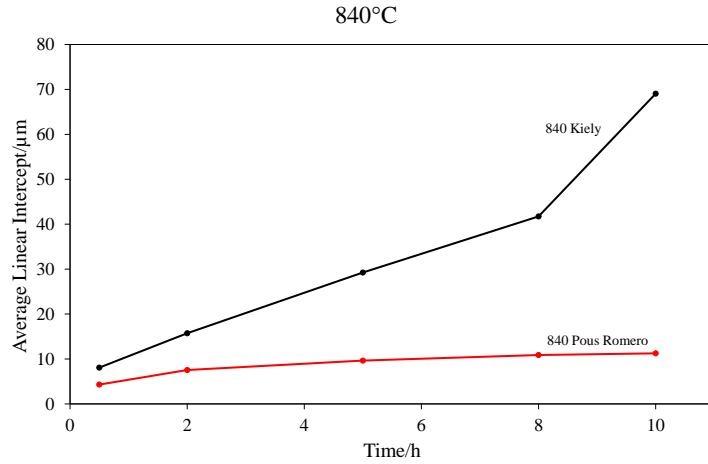
Figure 4.6: Grain size against holding time for 840°C for Grade 4N (black) and Grade 3 (red).
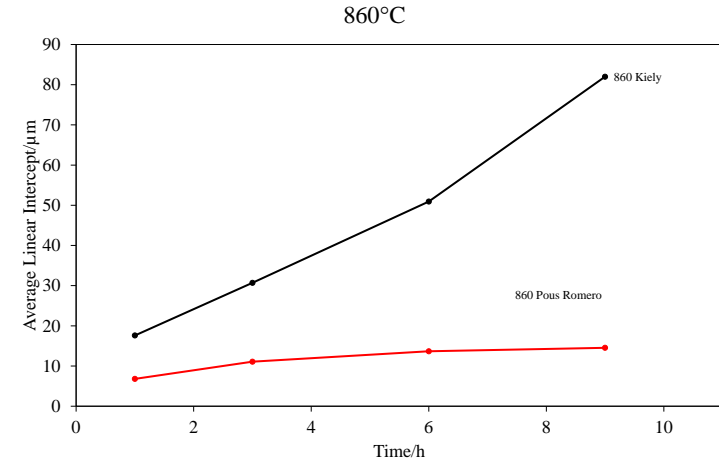
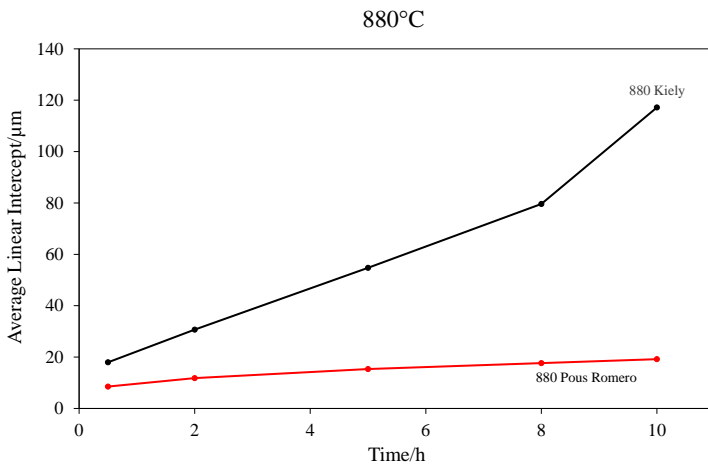Figure 4.7: Grain size against holding time for 860°C for Grade 4N (black) and Grade 3 (red).

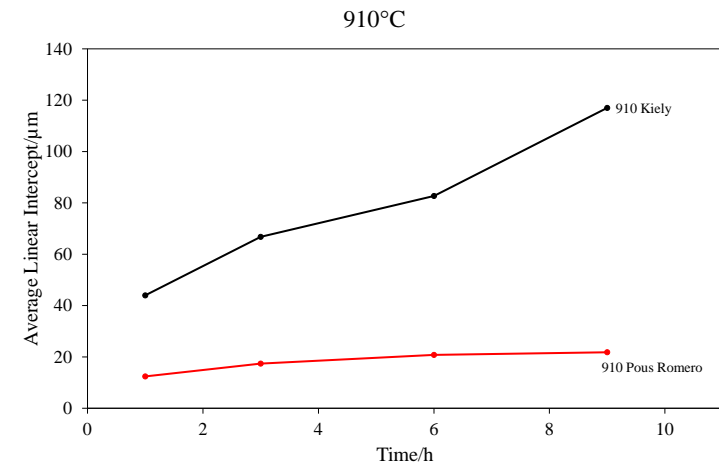Figure 4.8: Grain size against holding time for 880°C for Grade 4N (black) and Grade 3 (red).

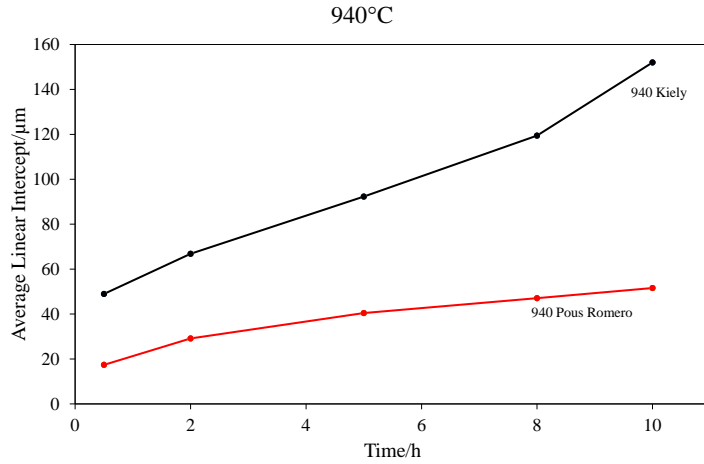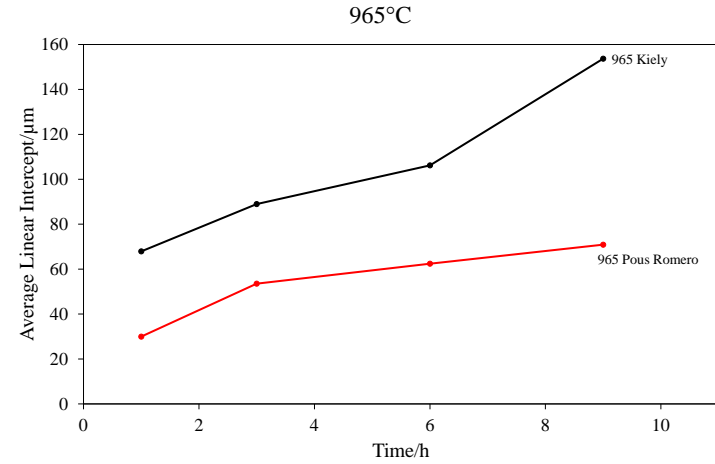Figure 4.9: Grain size against holding time for 910°C for Grade 4N (black) and Grade 3 (red).

Figure 4.10: Grain size against holding time for 940°C for Grade 4N (black) and Grade 3 (red).

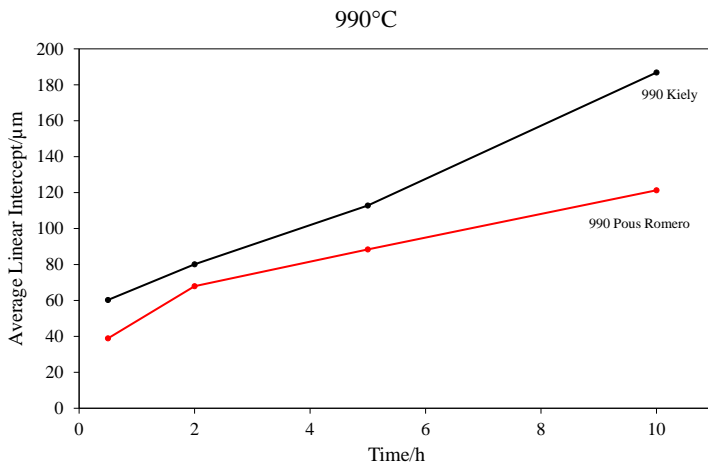Figure 4.11: Grain size against holding time for 965°C for Grade 4N (black) and Grade 3 (red).

Figure 4.12: Grain size against holding time for 990°C for Grade 4N (black) and Grade 3 (red).

4.1.2 Determination of austenite grain growth

Plots of frequency against mean linear intercept were plotted for all the austenisation temperatures and hold times. These graphs were utilised as a tool to conclude whether Grade 4N was undergoing uniform grain growth (Figure 4.13-4.19). These plots do not follow a Maxwell Boltzmann distribution and thus grain growth is not uniform and tends to be abnormal for all temperatures. Further discussion of this will take place in Section 5.
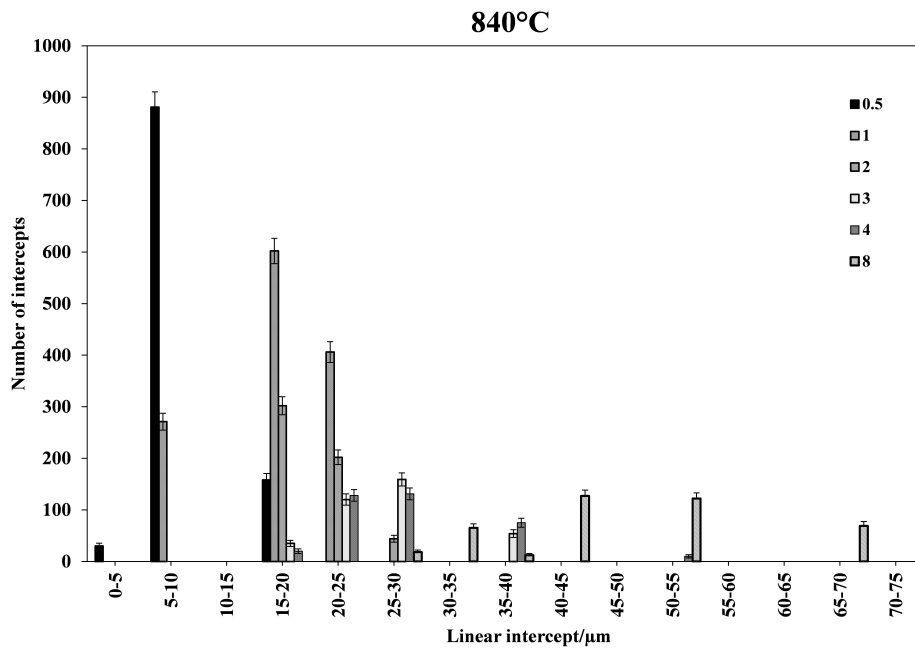
Figure 4.13: Linear intercept against number of intercepts for 840°C for Grade 4N for a selection of heat treatments.
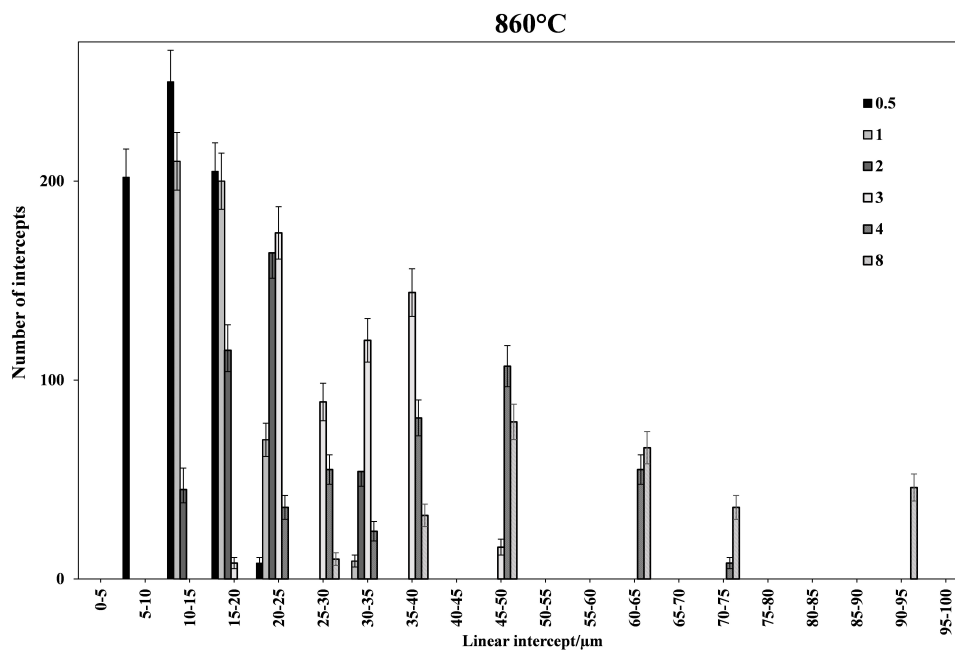

Figure 4.14: Linear intercept against number of intercepts for 860°C for Grade 4N for a selection of heat treatments.
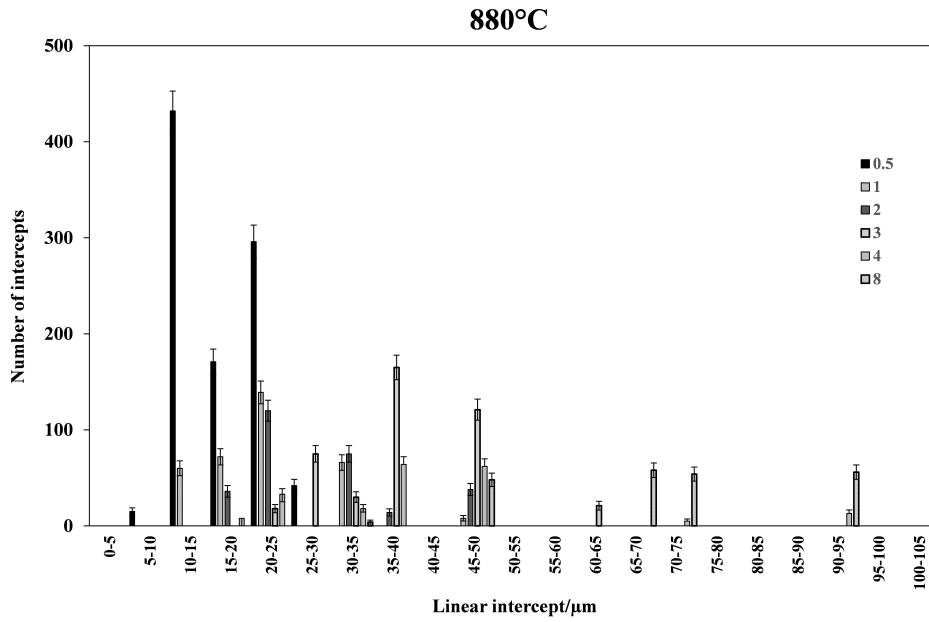
880°C

Figure 4.15: Linear intercept against number of intercepts for 880°C for Grade 4N for a selection of heat treatments.

910°C

Figure 4.16: Linear intercept against number of intercepts for 910°C for Grade 4N for a selection of heat treatments.

940°C

Figure 4.17: Linear intercept against number of intercepts for 940°C for Grade 4N for a selection of heat treatments.

965°C

Figure 4.18: Linear intercept against number of intercepts for 965°C for Grade 4N for a selection of heat treatments.

Figure 4.19: Linear intercept against number of intercepts for 990°C for Grade 4N for a selection of heat treatments.
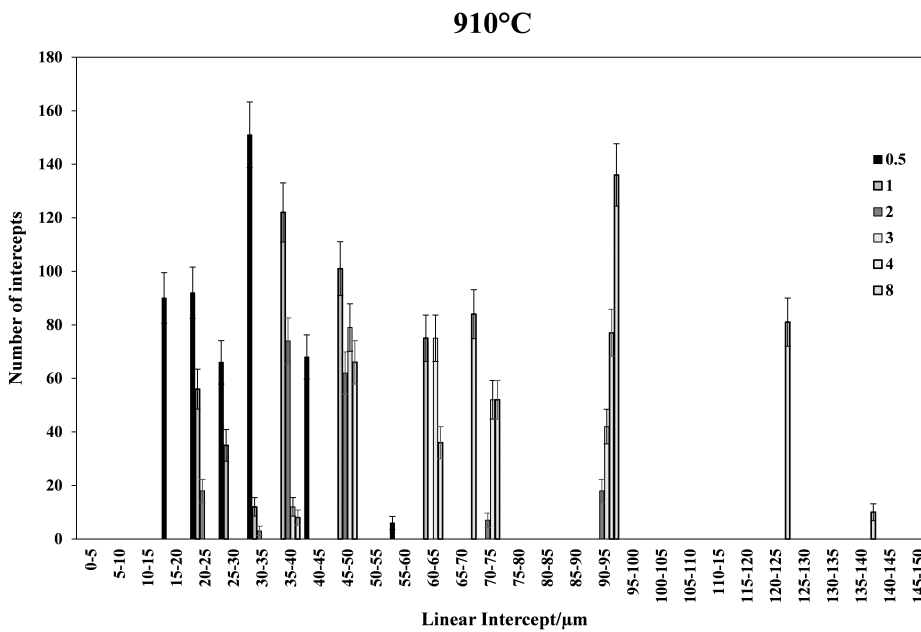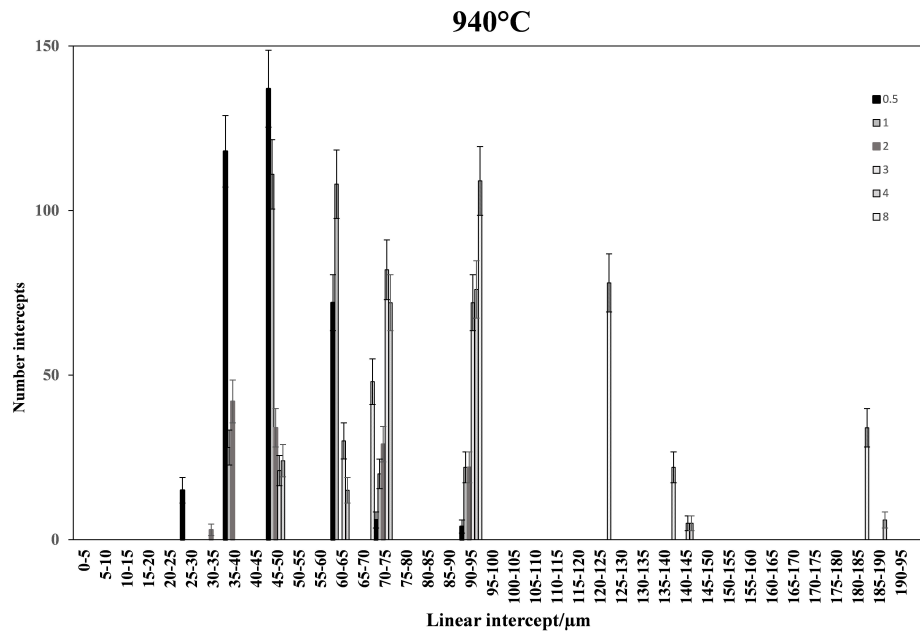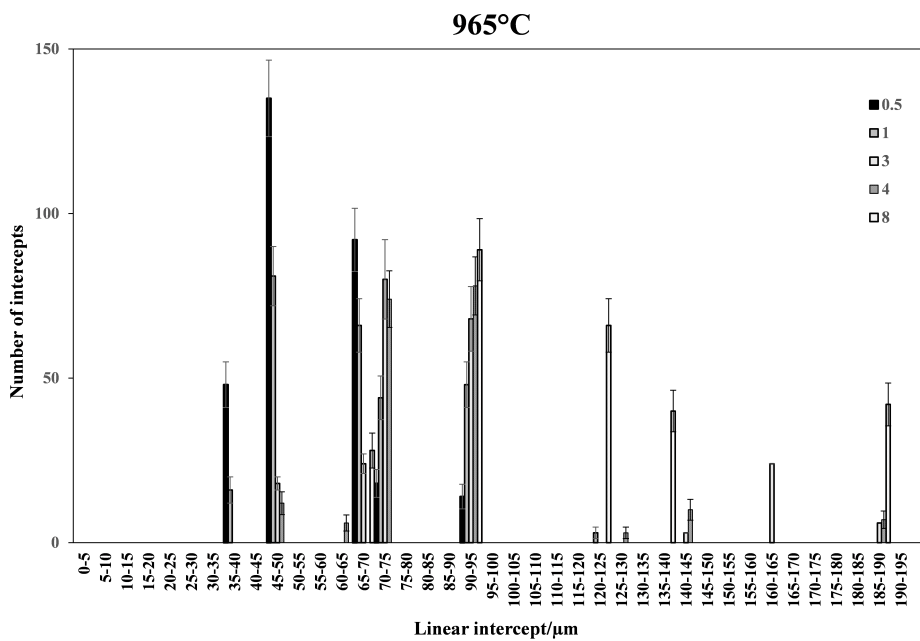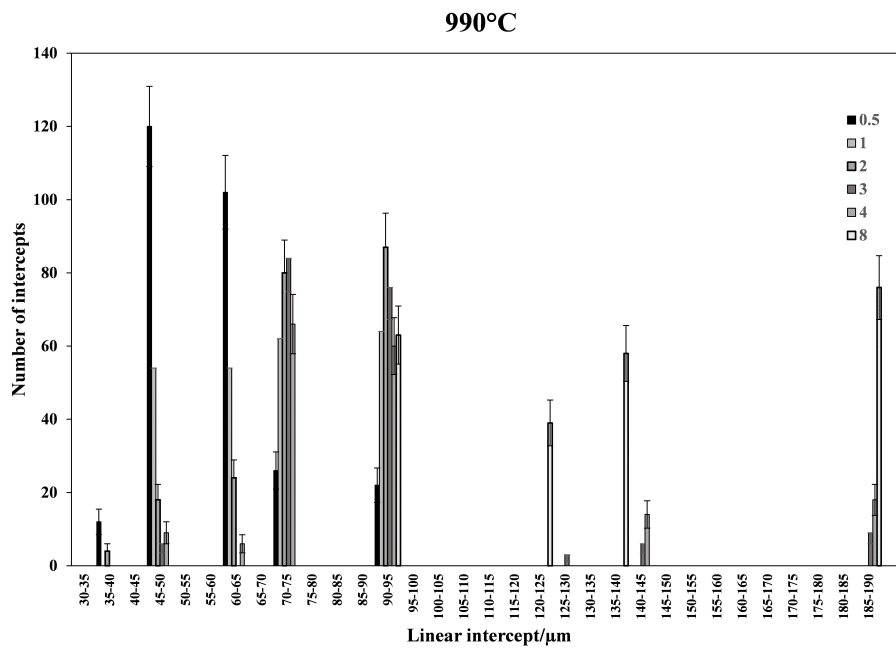
4.1.3 Microstructure

Micrographs were taken at 50 x magnification, using the Olympus BH microscope with a Leica DFC295 camera, in order observe grain structure formed upon thermal grooving. Examples of the microstructure are illustrated in Figure 4.20 clearly showing the grain boundaries.
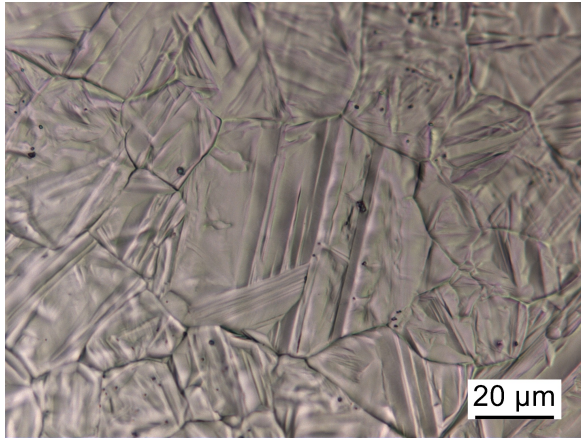
(a) Micrograph 880°C 4 hour hold time
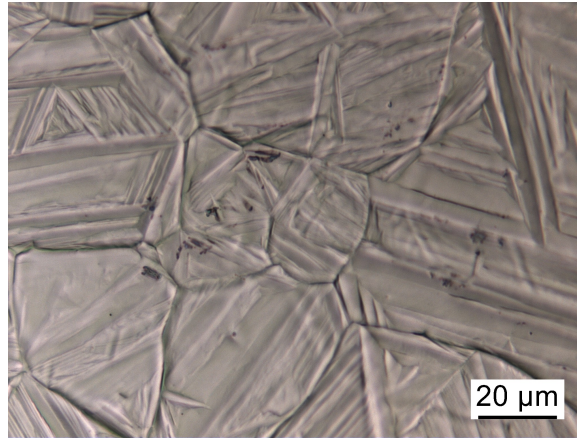
(b) Micrograph 910°C 4 hour hold time
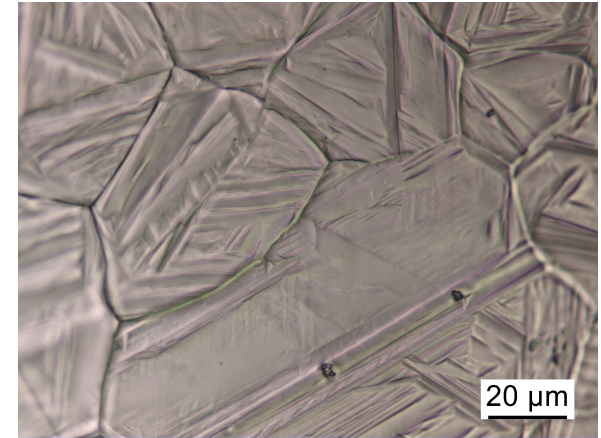
(c) Micrograph 940°C 4 hour hold time
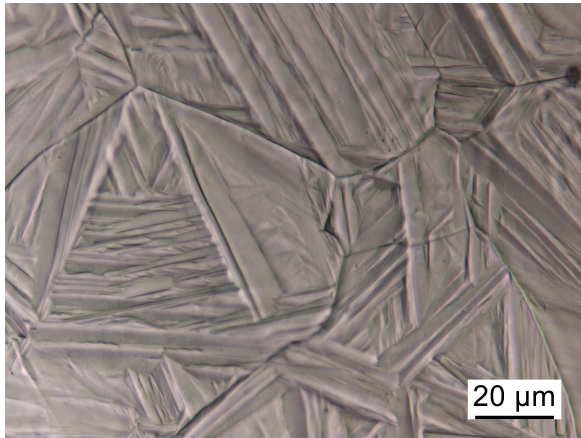
(d) Micrograph 965°C 4 hour hold time
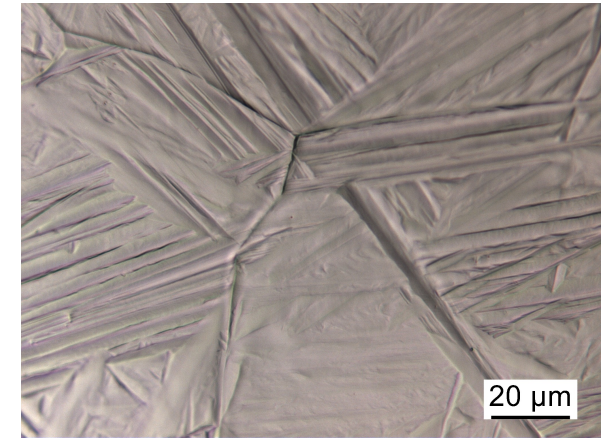
(e) Micrograph 990°C 4 hour hold time

Figure 4.20: Micrographs for varying austenitising temperatures with the same hold time

Further investigation of the microstructure was undertaken using the Phenox ProX SEM in Back Scattered mode with 15kV in order to see the martensite lathes. Figure 4.21 depicts the microstructure observed from the use of SEM.
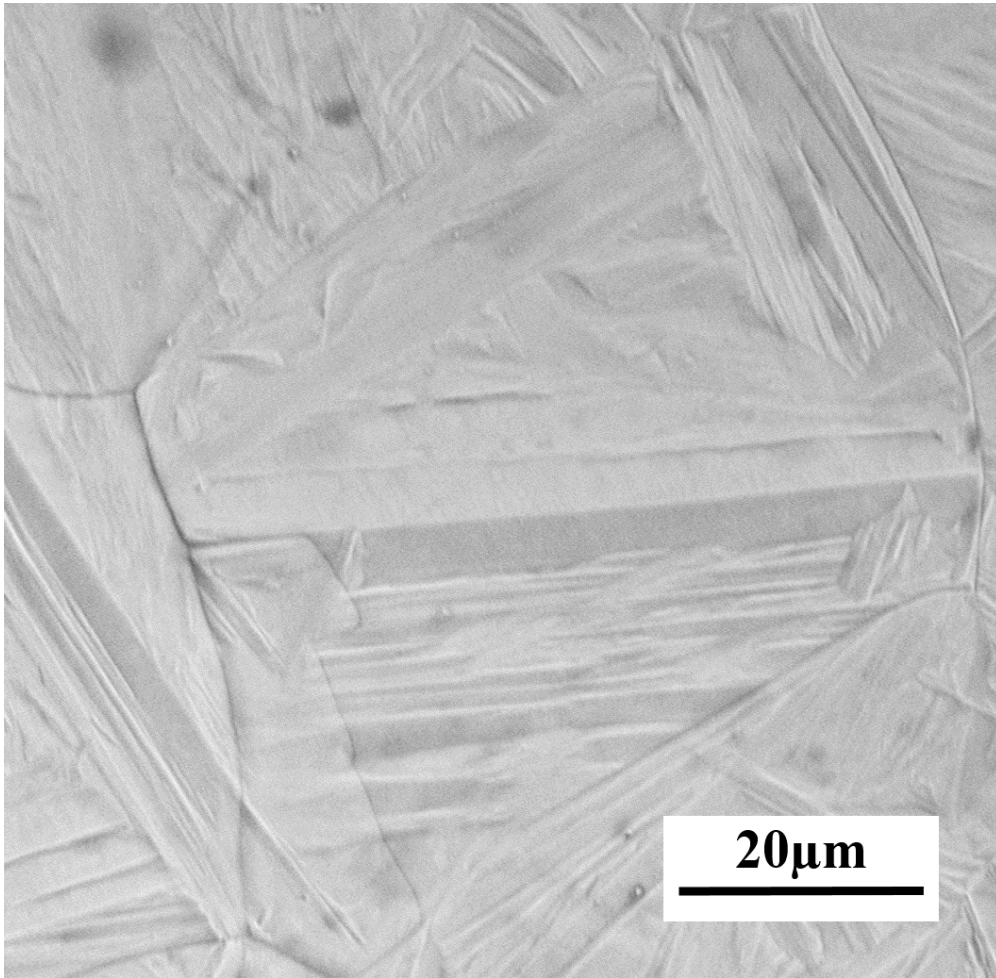
Figure 4.21: Back scattered image of microstructure for Grade 4N utilising the Phenom ProX SEM at 15kV.

5 — Discussion

As illustrated in Figure 4.1 there is the expected increase of austenite grain size for Grade 4N at all temperatures. The observed increase is monotonic except for the slight acceleration during heat treatment at 910°C. This is in contrast to the work by Pous-Romero [3] on the Grade 3 alloy which exhibits a sudden increase in grain size when AlN particles dissolve thereby reducing Zener drag leading to unrestrained grain growth. However, Grade 4N does not have significant pinning precipitates at the temperatures of interest. For example, pinning precipitate $M_{23}C_6$ [41-42] is estimated to be in solution at 757° C, based on MT-DATA calculations, and thus would not be expected to be present at the austenitising temperatures investigated in this report. This accounts for the grain growth phenomenon seen in Grade 4 whereby the grain size continues to increase with heat treatment time (Figure 4.1). Notably the lack of pinning precipitates could be due to the wide compositional differences between the two alloys.

When Grade 3 data are plotted along with those from Grade 4N it is clearly shown that Grade 3 undergoes a different austenite grain growth behaviour (Figure 4.2). With increasing hold times there is little increase in grain size for Grade 3 at low temperatures suggesting that the boundaries may be pinned by precipitated particles. At temperatures between 840°C and 910°C, moderate grain growth occurs for

Grade 3 with the values plateauing at longer hold periods . This is followed by an abrupt increase in growth rate at 940°C with the Grade 3 grain size doubling relative to samples held at lower temperatures.

Pous-Romero [3] proved that this sudden increase in grain growth at 940°C is due to the dissolution of aluminium nitride (AlN) particles (Figure 4.3). After which grain size continues to increase at higher temperatures, 990°C, and longer hold times and does not reach a limiting grain size within the scope of Pous-Romero's experimental research [3].

This is in contrast to Grade 4N which displays increased grain size with increasing hold times. The grain size for Grade 4N continues to increase as a function of time and temperature in the austenite phase field. Notably for experiments undertaken with the same heat treatment and hold times the grain size of Grade 4N is significantly larger, for example the grain size of Grade 4N was found to six times that of Grade 3 at lower temperatures prior to 940°C. This can be attributed to the weak boundary pinning and to a smaller volume fraction of pinning precipitates, as seen in Figure 4.3.

Equilibrium weight fraction calculations were undertaken using MT-DATA, based on the chemical compositions of Grades 3 and 4N, in order to compare the amount of AlN present. Figure 4.3 shows that Grade 3 contains approximately 1.75×10^{-2} wt% at 880°C, compared to Grade 4N which has a significantly smaller presence of AlN at this temperature, approximately 5×10^{-3} wt%. The absence of significant boundary pinning seen in Grade 4N can thus be related to the low fraction of pinning precipitates: AlN and $M_{23}C_6$, at the investigated austenitising temperatures but $M_{23}C_6$ found to be irrelevant in the in the austenite

phase field.

Comparison of calculated grain size and experimentally-measured grain size highlights that the unmodified model of Pous-Romero [3] is able to estimate the Grade 4N grain size at lower temperatures and low hold times (Figure 4.4). However as the temperature increases along with the hold time the calculated grain size becomes less accurately predicted for Grade 4N. The FORTRAN code developed as a predictive tool by Pous-Romero et al. [3,43] is for alloys which undergo pinning, meaning that at longer hold times for Grade 4N and for Grade 3 it becomes less accurate due to reduced pinning effect in both alloys. However it should be noted that value for the activation energy, Q, was based on previous literature and may not be the correct value for the growth kinetics of grade 4N. The value of Q for Grade 4N could be incorrect due to the broader compositional difference between Grade 3 and Grade 4N. The value of Q was previously stipulated as $190 \, \text{kJ} \, \text{mol}^{-1}$ based on experimental data being interpreted to avoid overfitting [3]. In this case Q, the activation for grain growth, may be a lower value as grain growth is significant from the start and does not seem to have to overcome a pinning force at the start. Thus Q needs investigation in order to deduce if it is the most correct value with regard to Grade 4N.

Pous-Romero et al. showed that Grade 3 displays a homogenous distribution of grain sizes at temperatures between 840°C to 910°C (Figure 4.5). Figures 4.6 - 4.12 compare the grain sizes at selected holding times and temperatures for Grade 3 and Grade 4N. It is evidenced that there is a significant difference in grain size measurements at the low temperatures. Thus figures 4.6 to 4.12 provide further evidence that at low temperatures the grain growth for Grade 3 is being dominated by pin-

ning precipitates whereas Grade 4N displays significantly larger grain size. At 940°C, Figure 4.10, the grain size for Grade 3 and Grade 4N begins to converge. This convergence continues to occur at higher temperatures. Findings by Pous-Romero et al [3] concluded that at temperatures above 940°C the grain size distribution for Grade 3 changes from uniform to bimodal [3] (Figure 4.5). This change in grain distribution at higher temperatures was attributed to the reduction in the volume fraction of AlN pinning precipitate. Specifically, at sufficiently high temperatures, the localised pinning forces were reduced due to the heterogenous dissolution of the nitrides. Another possibility is that solute drag is occuring which requires further investigation.

In comparison the grain size distributions for Grade 4N, figures 4.12-4.18, show that at low temperatures the grain size distribution is broadly normal distributed; with only a slight increase in temperature and hold time causing a bimodal distribution to be apparent. The bimodal nature of grain size can be attributed to a reduction in localised pinning forces [3]. This could be due to microsegregation occuring further investigation of this is required.

The micrographs presented in Figure 4.20, demonstrate also that Grade 4N does not display normal grain growth; showing that the grain size varies across all temperatures with larger grains sitting next to smaller grains thus confirming abnormal grain growth. These micrographs illustrate the thermal grooves which have formed upon holding at the austenitising temperature. It should be noted that surface relief is apparent at all of these temperatures with it being emphasised at high temperatures due to the coarsening on the plates. Literature has stipulated that as the austenite grain mobility decreases the higher the inter-

ference of the grooves with the surface motion of the grain boundaries [55].A possible reason as to the bimodal nature is potential interdendritic segregation.

Further images were taken from the sample heat treated at the highest temperature 990°C (Figure 4.21). It can be seen that there is martensite present within the austenite grain. Significant surface relief is associated with this lath which stops at the grain boundary. This surface relief occurs below the martensite start temperature. Thus it can be deduced that the austenite grain boundaries have not moved away from the grooves and as such truly reflects the grain size at the heat treatment temperature.

Overall, it can be concluded from the results thus far that austenite grain boundaries in Grade 4N are not hindered by pinning particles, unlike Grade 3. However further research into the microstructure of this alloy is going to be crucial in order to confirm that this is the case.

5.1 Implication of this research

The austenite grain size has a significant effect on the mechanical properties. Notably toughness decreases with increasing grain size this is a crucial property with regard to fracture. Thus a fine microstructure, that is a smaller grain size, is desirable in order to increase toughness [64-66].

As the austenite grains grow the amount of martensite transformed increases. This is explained by Prawoto *et al.* [67] based on Fischer's work whereby the volume fraction of martensite is proportional to the cube

of the austenite grain size. It was found that larger austenite grains needed little undercooling below M_S in order to detect a martensite volume fraction. Notably less bainite and ferrite are formed when the grain size increases as there are fewer grain boundary nucleation sites per unit volume [67,68]. Thus large grain size leads to an increase in hardenability.

Overall the implications of this research have shown that careful consideration of heat treatment is required for Grade 4N. This is due to the nature of the grain growth phenomenon in Grade 4N whereby small changes in heat treatment time causes significant increases in grain size. Thus further research is needed in order to determine the optimal hold time and temperature in order to gain the desired microstructure and thus properties.

5.2 Future work

Based on the experimental findings of this report further research is required in order to investigate the exact microstructure of Grade 4N in order to deduce whether any pinning mechanisms are involved. This will be valuable to the industrial community in order to optimise heat treatment processes of this alloy to gain the desired microstructure and thus optimise the properties for pressure vessel steels.

An intriguing phenomenon is that the curves in Figure 4.1 do not have a common origin. Thus dilatometry experiments and predictive models should be used to see if there is a common origin.

Additional calculations of grain size between the Ac_3 temperature and the chosen austenitsation temperature should be undertaken with different heating rates relevant to RPV dimensions used in the marine sector. This will aid the ability to deduce the optimum heat treatment based on industrial criteria. Calculations should be utilised in order to show there is little effect on grain size evolution during cooling from austenitisation temperature down to Ae_3.

Consideration of what is valuable to the manufacturers and end users should be considered. Further development of CCT, TTT curves for Grade 4N would be useful in order to establish the resultant microstructures from the proposed heat treatments. Additional investigation should be undertaken in order to deduce if these microstructures can be accurately generated from the modelling approaches utilising MTData. It should be noted that researchers need to utilise these thermodynamic models with care as they are mainly based on binary alloys. Thus these

alloys should be utilised in balance as a tool to make predictions noting that the specific heat should be measured rather than predicted.

Mechanical properties experiments would also be desirable so as to conclude whether Grade 4N is the ideal candidate alloy for implementation in the new generation of nuclear reactors.

6 — Conclusions

Overall the general objective of this research project was to investigate the austenite grain growth of SA508 Grade 4N. Notably this research project has shown for the first time the austenite grain growth behaviour of Grade 4N is significantly different to Grade 3 steel currently utilised in RPVs.

However, whereas significant investigation of pinning mechanism of Grade 3 has been carried, there is little information with regard to the pinning in Grade 4N. It was deduced through this research that there were limited pinning mechanisms occurring at the chosen austentisation temperatures. Significantly Grade 4N grains continued to grow with increasing austentisation temperature and hold time. One of the hypothesised reasons for this alloy not displaying pinning mechanism was due to a lower fraction of AlN pinning particles present along with the dissolution of $M_{23}C_6$. This hypothesis was able to be evidenced by MTDATA calculations carried out and was reflected in experimental results. Future work should include the use of synchrotron in order to gain an insight into the microstructure via the use of diffraction patterns and thus whether the AlN precipitates play any role in pinning or are indeed in too lower fraction to be effective.

Through the use of dilatometry in order to produce thermal grooving

the grain sizes were able to be measured. Experimental evidence clearly illustrated that for Grade 4N, grains are considerably larger and displayed a bimodal nature. This phenomenon was also reflected at high temperature and long hold times in the Grade 3 investigations carried out by Pous-Romero [3].

Through the use of microscopy the thermal grooves were able to be observed with more prominent grooves at higher temperatures. With high temperature Grade 4N austenite grains displayed increased relief and higher martensite fraction. This can be related to literature whereby it has been concluded that with increasing austenite grain size there is increased martensite lathes. The SEM image taken after a heat treatment at 990°C highlighted that the martensite lath formed and the surface relief, having been formed below the martensite start temperature, stop at the grain boundary and thus reflect the grain size at the heat treatment temperature.

With minimal literature having been published on the austenite growth behaviour for Grade 4N this research is a significant foundation from which further investigations need to be carried out. Future aims should be to deduce a heat treatment for fabrication of an optimised microstructure and properties for application as an RPV.

Bibliography

[1] D. Bodansky, *Nuclear Energy: Principle, Practices and Prospects*, New York: American Institute of Physics, 1996, pp. 25-54,

[2] E. Rutherford, "Radioactivity", in *The Encyclopaedia Britannica*, 11th ed., New York: The Encyclopaedia Britannica Company, 1910, p. 802

[3] H. Pous-Romero, "Quantitative basis for the structure and properties of a critically-important pressure vessel steel", Ph.D. Thesis , Department of Materials Science and Metallurgy, University of Cambridge, Cambridge, 2014

[4] J.M. Bodansky, *Nuclear power, a very short introduction*, Oxford: Oxford University Press, 2011, pp. 25-54

[5] C. Weiner, "1932 - Moving into the New Physics, in *History of Physics*, S.R.Weart and M.Phillips eds., New York: American Institute of Physics, 1985

[6] E. Segre, *From X-rays to Quarks: Modern Physicists and Their Discoveries*, San Francisco: W. H. Freeman, 1980

[7] R. Rhodes, *The Making of the Atomic Bomb*, USA: Richard Rhodes, 1986

[8] R. Tilbrook, "Chapter 3- Early History of Nuclear Energy" in *Nuclear energy encyclopedia: science, technology and applications*,

T.B. Kingery, S.B. Krivit and J.H. Lehr , Eds., Oxford: Wiley-Blackewell, 2011, pp. 23-29

[9] D. Cooper, *Enrico Fermi: And the Revolutions in Modern physics*, Oxford University Press, 1999

[10] D. Kvasnicka, *The history of nuclear energy*, U. S. Department of Energy, 2011

[11] "Enrico Fermi", Encyclopaedia Britannica, Encyclopaedia Britannica Inc, [Online]. Available at: https://www.britannica.com/biography/Enrico-Fermi [Accessed: August 11, 2016]

[12] Prof W.M. Stacey, "Chapter 1- Neutron Nuclear Reactions", in *Nuclear Reactor Physics Second Edition*, Second Edition, Wiley-VCH Verlag GmbH & Co. KGaA, Weinheim, Germany, 2007

[13] E.E. Lewis, "Chapter 1-Nuclear Reactions", in *Fundamentals of Nuclear Reactor Physics*, Amsterdam: Academic Press, 2008

[14] F. Close, "Chapter 2-Nuclear Alchemy", in *Nuclear Physics: A Very Short Introduction*, Oxford: Oxford University Press, 2015

[15] K. Henwood and N. Pidgeon, "Chapter 5-Gender, ethical voices, and UK nuclear energy in the post-Fukushima era", in *The Ethics of Nuclear Energy: Risk, Justice, and Democracy in the post-Fukushima Era*, B. Taebi and S. Roeser Eds, Cambridge: Cambridge University Press, 2015

[16] C. Butler, K.A. Parkhill and N. Pidgeon, *Deliberating Energy System Transitions in the UK Transitions in the UK*, UKERC, London, 2013

[17] *The Carbon Plan: Delivering our low carbon future*, Department of Energy and Climate Change, London, 2011

[18] International Atomic Energy Agency, "Nuclear Power Reactors in the World",in *Reference Data Series No. 2*, IAEA, Vienna, 2014

[19] I.N. Kessides (August 2010), "Nuclear Power: Understanding the economic risks and uncertainities",in *Energy Policy*, Vol. 38(8), pp. 3849-3864

[20] J.G. Marques (September 2010), "Evolution of nuclear fission reactors: Third generation and beyond", in *Energy Conversion and Management*, Vol. 51(9), pp. 1774-1780

[21] A.M. Weinberg,*The First Nuclear Era: The Life and Times of a Technological Fixer*, American Institute of Physics, New York, 1994

[22] R.L. Murray, Nuclear Energy: *An Introduction to the Concepts, Systems, and Applications of Nuclear Processes*, Sixth Edition. Butterworth-Heinemann, Burlington, MA, 2009, pp. 323337

[23] International Atomic Energy Agency, "Nuclear Power Reactors in the World",in *Reference Data Series No. 2*, IAEA, Vienna, 2009

[24] W.M. Stacey, *Nuclear Reactor Physics*, 2nd Ed. Wiley-VCH, Weinheim, Germany, 2007, pp. 249250

[25] U.S. Nuclear Regulatory Commission,"A graphic illustrating the typical pressurized -water reactor process", [Online]. Available at: https://www.flickr.com/photos/nrcgov/10713724664/ [Accessed: August 11, 2016]

[26] T.L. Dickson and S.N.M. Malik,"An updated probabilistic fracture mechanics methodology for application to pressurized ther-

mal shock", in *International Journal of Pressure Vessels and Piping*, 2001, Vol. 78 (2:3), pp. 155163

[27] K-H Lee, M.J. Jhung, M-C Kim and B-S Lee"Effects of tempering and PWHT on microstructures and mechanical properties of SA508 Gr. 4N Steel, in *Nuclear Engineering and Technology*, 2014, Vol. 46 (3), pp. 413-422

[28] B-S Lee, M-C Kim, M.J. Jhung and J.H. Hong "Characterization of high strength and high toughness Ni-Mo-Cr low alloys steels for nuclear application, in *International Journal of Pressure Vessels and Piping*, 2010, Vol.87 (1), pp. 74-80

[29] K-H Lee, M-C Kim, B-S Lee and D-M Wee "Analysis of the master curve approach on the fracture toughness properties of SA508 Gr.4N NiMoCr low alloy steels for reactor pressure vessels, in *Materials Science and Engineering A*, 2010, Vol. 527 (15), pp. 3329-3334

[30] ASTM, *Standard Specification for Quenched and Tempered Vacuum Treated Carbon and Alloy Steel Forgings for Pressure Vessels A 508/A 508M*, 2004

[31] K-H Lee, S-G Park, M-C Kim, B-S Lee and D-M Wee "Characterization of transition behaviour in SA508 Gr.4N Ni-Cr-Mo low alloy steels with microstructural alteration by Ni and Cr contents, in *Materials Science and Engineering A*, 2011, Vol. 529, pp. 156-163

[32] E.G. Nisbett, "Chapter 17- Steel Forgings for the Pressure Vessel Industry" in *Steel Forgings: Design, Production, Testing and Applications*, USA: ASTM International, 2005, p. 103

[33] S.J. Zinkle and G.S. Was, "Materials challenges in nuclear energy", in *Acta Materialia*, 2013, Vol. 61(3), pp. 735-758

[34] https://www.euronuclear.org/info/encyclopedia/r/reactor-pressure-vessel.htm. (2015)

[35] Y. Tanaka, "Development of high purity large forgings for nuclear power plants", in *Journal of Nuclear Materials*, 2011, Vol. 417 (1:3), pp. 854-859

[36] D.J. Cogswell, "Statistical Modelling of the Transition Toughness Properties of Low Alloy Pressure Vessel Steels Volume 1: Main Body", Ph.D. Thesis , Department of Metallurgy and Materials, School of Engineering, The University of Birmingham, Birmingham, 2010

[37] J. Talamantes-Silva, P. Bates, S. Al-Bermani, P. Davies, A. Hambleton and D. Bunney, "New challenges in the production of ultra large forgings for the manufacturing of pressure vessels", in *Proceedings of the ASME 2013 Pressure Vessels and Piping Conference*, 2013, Paris

[38] E.J. Pickering, "Macrosegregation in Steel Ingots", PhD Thesis, Department of Metallurgy and Materials, The University of Cambridge, Cambridge, 2014

[39] H. Kakimoto, T. Arikawa, Y. Takahashi, T. Tanaka, and Y. Imaida, "Development of forging process design to close internal voids", in *Journal of Materials Processing Technology*, 2010, Vol. 210 (3), pp. 415-422

[40] Y. Tanaka and I. Sato, "Development of high purity large forgings for nuclear power plants", in *Journal of Nuclear Materials*, 2011, Vol. 417 (1-3), pp. 854-859

[41] P. Bocquet, A. Cheviet, and R. Dumont, "Examples of the evolution of materials for nuclear applications: metallurgical improve-

ment of 16MND5 steel and new technologies for manufacturing heavy components", in *Nuclear Engineering and Design*, 1994, Vol. 151 (2-3), pp. 503-511

[42] K-H Lee, M-C Kim, B-S Lee and D-M Wee,"Master curve characterization of the fracture toughness behavior in SA508 Gr.4N low alloy steels", in *Journal of Nuclear Materials*, 2010, Vol. 403 (1-3), pp. 68-74

[43] Y.R. Im, Y.J. Oh, B.J. Lee, J.H. Hong, and H.C. Lee,"Eects of carbide precipitation on the strength and charpy impact properties of low carbon Mn-Ni-Mo bainitic steels", in *Journal of Nuclear Materials*, 2001, Vol. 297(2), pp. 138-148

[44] H Pous-Romero and H Bhadeshia,"Coalesced Martensite in Pressure Vessel Steels", in *Journal of Pressure Vessel Technology*, 2014, Vol. 136 (3)

[45] C.M. Sellars and J.A. Whiteman,"Recrystallization and grain growth in hot rolling", in *Material Science and Technology*, 1979, Vol. 13 (3-4)

[46] L. Vanherpe, N. Moelans, B. Blanpain and S. Vandewalle," Pinning effect of spheroid second-phase particles on grain growth studied by three-dimensional phase-field simulations", in *Computational Materials Science*, 2010, Vol. 49(2), pp. 340-350

[47] H.R. Wang and W. Wang. "Simple model for austenite grain growth in microalloyed steels", in *Materials Science and Technology*, 2008, Vol. 24(2), pp. 228232

[48] I. Andersen and Ø. Grong "Analytical modelling of grain growth in metals and alloys in the presence of growing and dissolving

precipitates- I. Normal grain growth", in *Acta Metallurgica et Materialia*, 1995, Vol. 43, pp. 2673-2688

[49] S. Lee and Y. Lee "Prediction of austenite grain growth during austenitization of low alloy steels", in *Materials and Design*, 2008, Vol. 29, pp. 1840-1844

[50] Y. Palizdar, D. San-Martin, M. Ward, R.C. Cochrane, R. Brydson and A.J. Scott "Observation of thermally etched grain boundaries with the FIB/TEM technique", in *Materials Characterization*, 2013, Vol. 84, pp. 28-33

[51] W.W. Mullins " Theory of Thermal Grooving", in *Journal of Applied Physics*, 1957, Vol. 28, p. 333

[52] D. Xia, C. Zhou, Y. Liu, J. Wang, C. Fu, K. Wang and M. Li "Mechanical Properties and Corrosion Resistance of SA508-4 Low Carbon Alloy Steel", in *Electrochemistry*, 2013, Vol. 81, pp. 262-268

[53] M.G. Burke, R.J. Stofanak, J.M. Hyde, C.A. English and W.L. Server "Microstructural Aspects of Irradiation Damage in A508 Gr 4N Forging Steel: Composition & Flux Effect,", in *ASTM*, 2004, Vol. 1

[54] S-G. Park, K-H. Lee, K-D. Min, M-C. Kim and B-S. Lee "Characterization of phase fractions and misorientations on tempered Bainitic/Martensitic Ni-Cr-Mo low alloy RPV steel with various Ni content", in *Metals and Materials International*, 2013, Vol. 19 (1), pp. 49-54

[55] Y-S. Ahn, H-D. Kim, T-S. Byun, Y-J. Oh, G-M. Kim and J-H. Hong " Application of intercritical heat treatment to improve toughness

of SA508 Cl.3 reactor pressure vessel steel", in *Nuclear Engineering and Design*, 1999, Vol. 194 (2-3), pp. 161-177

[56] G.E.Dieter, *Mechanical Metallurgy*, London: McGraw-Hill Book Company, 1988, pp. 184-191

[57] H.K.D.H.Bhadeshia and R.W.K.Honeycombe, *Steels Microstructure and properties*, 3rd edition, Amsterdam: Butterworth Heinemann Elsevier, 2010, pp. 17-32

[58] W. Rosenhain, "The Hardness of Solid Solutions", *Proceedings of the Royal Society of London*, 1921, Vol. 99, pp. 196-202)

[59] F.R.N. Nabarro, "The Mechanical Properties of Solid Solutions",*Proceedings of the Royal Society of London*, 1946, Vol. 58, pp. 669-676

[60] R.I. Fleischer, "Solution Hardening",*Acta Metallurgica*, 1961, Vol. 9, pp. 996-1000

[61] R.I. Fleischer, "Substitutional Solution Hardening",*Acta Metallurgica*, 1963, Vol. 11, pp. 203-209

[62] H. Gleiter and E. Hornhogen, " Beobachtung der Wechselwirkung von Versetzungenmit Koh arenten Geordneten Zonen (II)",*Physica Statu Solidi*,1965, Vol. 12, pp. 251-264

[63] ASTM. *ASTM E112-13 Standard Test Methods for Determining Average Grain Size*, ASTM International, West Conshohocken, PA, 2013, Available at: http://dx.doi.org/10.1520/E0112 [Accessed at: August 11, 2016]

[64] C.A. Schneider, W.S. Rasband and K.W. Eliceiri, "NIH Image to ImageJ:25 years of image analysis", in *Nature methods*, 2012, Vol. 9 (7), pp. 671-675

[65] C García de Andrés, F.G. Caballero, C. Capdevilla and D. San Mart 'in, "Revealing austenite grain boundaries by thermal etching: advantages and disadvantages", in *Materials Characterization*, 2002, Vol. 49 (2), pp. 121-127

[66] J. Otubo, F.C. Naciment, P.R. Mei, L.P. Cardoso and M.J. Kaufman, "Influence of Austenite Grain Size on Mechanical Properties of Stainless SMA", in *Materials Transactions*, 2002, Vol. 43 (5), pp. 916-919

[67] Y. Prawoto, N. Jasmawati and K. Sumeru, "Effect of Prior Austenite Grain Size on the Morphology and Mechanical Properties of Martensite in Medium Carbon Steel", in *Materials Science and Technology*, 2012, Vol. 28 (5), pp. 461-466

[68] H-S. Yang and H.K.D.H. Bhadeshia, "Austenite Grain Size and Martensite-Start Temperature", in *Scripta Materialia*, 2009, Vol. 60 (7), pp. 493-495